Journal of Materials Chemistry C

High performance organic second- and third-order nonlinear optical materials for ultrafast information processing

Journal:	*Journal of Materials Chemistry C*
Manuscript ID	TC-REV-07-2020-003224.R1
Article Type:	Review Article
Date Submitted by the Author:	20-Aug-2020
Complete List of Authors:	Wu, Jieyun; University of Electronic Science and Technology of China, Li, Zhong'an; Huazhong University of Science and Technology, Chemistry and Chemical Engineering Luo, Jingdong; City University of Hong Kong, Department of Chemistry; City University of Hong Kong, Shenzhen Research Institute Jen, Alex; University of Washington, Materials Science and Engineering; University of Washington, Chemistry

SCHOLARONE™
Manuscripts

ARTICLE

High performance organic second- and third-order nonlinear optical materials for ultrafast information processing†

Received 00th January 20xx,
Accepted 00th January 20xx

DOI: 10.1039/x0xx00000x

Jieyun Wu*[a, b], Zhong'an Li*[c], Jingdong Luo*[a] and Alex K-Y Jen*[a, d]

Organic nonlinear optical (NLO) materials are very important for high-speed information processing in addressing the challenges of reduced energy consumption, and enhanced speed and bandwidth. In particular, organic second-order NLO materials are very promising for meeting the combined requirements of ultra-low energy and ultra-high bandwidth in electro-optic (EO) modulation, while organic third-order NLO materials have good potential for applications in ultra-speed all-optical signal processing (AOSP). This review highlights recent significant progresses made in organic second- and third-order NLO materials. For second-order NLO materials, the recent advances in efficient and cost-effective synthesis of dipolar polyene chromophores and thin-film engineering for efficient electric field poling are summarized. The applications and prospects of these high-performance EO materials are also discussed. For third-order NLO materials, we discuss the molecular design strategies of cyanine dyes for AOSP applications, particularlly focusing on anionic tricyanofuran (TCF)-based cyanines. We aim to provide a better understanding of strcuture-property relationships for cyanine-based AOSP materials. At last, a summary and outlook for advancing high-performance organic NLO materials are provided.

1. Introduction

With global internet traffic grows by exponential rate, the digital traffic jams threaten to throttle the information technology revolution.[1, 2] Current network is far from ready for the era of information explosion due to new emerging technologies such as big-data, cloud computing, autonomous vehicles, virtual reality and high-definition video *etc*.[3] There is an urgent need in constructing transformative photonic devices with ultra-low energy consumption, ultra-large bandwidth, and ultra-high speed for data centers, metro networks and supercomputing facilities.[4] Undoubtedly, this challenge requires the synergetic innovation from fundamental chemistry in photonic materials to device engineering and the further construction of communication systems.

There is overwhelming evidence that organic nonlinear optical (NLO) materials play a critical role in the development of photonic platforms.[5-12] Successful deployment of organic second-order NLO (or organic electro-optic, EO) polymers have contributed significantly to photonic applications.[13-19] Plasmonic-organic hybrid (POH) modulators with organic EO materials take advantage of silicon photonics, organic electro-optics and plasmonic sub-wavelength light confinement, and meanwhile they overcome both the speed limitations of electronics and photonics of efficient EO modulation on micrometer footprints.[20-24] POH EO modulators with energy consumption as low as 30 fJ/bit have been fabricated in a single metal layer.[25] The POH in-phase/quadrature (IQ) electro-optic modulators exhibited ultra-low energy consumption at attojoule per bit (0.07 fJ/bit at 50 Gbit/s, or 0.3 fJ/bit at 200 Gbit/s).[26] The proof-of-concept THz-to-optical conversion in 16 m wireless communications using an ultra-broadband POH EO modulator with a 3-dB bandwidth of 0.36 THz (360 GHz) was successfully demonstrated.[27] Silicon-organic hybrid (SOH) EO modulators show comprehensive performance improvement on bandwidth (>100 GHz), half-wave voltage ($V\pi$<1 V) and optical loss on millimeter footprints.[28-34] The innovation in device structure such as silicon slot waveguide, photonic crystal waveguide, and micro-ring resonator combining highly efficient and stable EO materials has significantly advanced the progress of CMOS-compatible active photonic devices for coherent optical communication.[29, 35-40] Hybrid polymer EO modulator using Sol-Gel conductive cladding is exceptionally promising in high-bandwidth and low-$V\pi L$ EO modulation.[41-47]

Organic third-order NLO materials are an intriguing materials for all-optical signal processing to realize very high speed optical switching and modulation.[48-51] The silicon-organic hybrid waveguides with bandwidths exceeding 100 Gbit/s by integrating organic NLO materials have been achieved. Recently, silicon–organic hybrid waveguide with a record nonlinearity coefficient of $\gamma \approx 1\times10^5$ $W^{-1}km^{-1}$ and all-optical

[a] *Department of Chemistry and Shenzhen Research institute, City University of Hong Kong, Kowloon 999077, Hong Kong SAR, China. E-mail: jingdluo@cityu.edu.hk, alexjen@cityu.edu.hk.*
[b] *School of Optoelectronic Science and Engineering, Key Lab of Optical Fiber Sensing and Communication (Ministry of Education), University of Electronic Science and Technology of China, Chengdu 611731, China. Email: jieyunwu@uestc.edu.cn.*
[c] *Key Laboratory for Material Chemistry of Energy Conversion and Storage (Ministry of Education), School of Chemistry and Chemical Engineering, Huazhong University of Science and Technology, Wuhan 430074, China. Email: lizha@hust.edu.cn.*
[d] *Department of Material Science and Engineering, City University of Hong Kong, Kowloon 999077, Hong Kong SAR, China.*
† *Dedicated to Professor Tobin J. Marks on the occasion of his 75th birthday.*
Electronic Supplementary Information (ESI) available: [details of any supplementary information available should be included here]. See DOI: 10.1039/x0xx00000x

demultiplexing of 170.8 Gbit/s to 42.7 Gbit/s was performed in all optical signal processing.[52] In addition, third-order NLO materials can also be used for three-dimensional (3D) micro- and nanofabrication by taking advantage of two-photon or multiphoton absorption.[53]

Overall, the improvement in NLO effect of organic materials together with the systematic design and engineering in POH, SOH, Sol-gel Hybrid and all-polymer waveguide devices has resulted in a substantial and significant progress in device performance, including energy consumption at the level of attojoule per bit, V_π lower than 0.5 V, bandwidth of higher than 300 GHz, signal processing speed of higher than 200 Gb/s and device footprints on the order of μm^2. It should be noted that, without the endeavours from the researchers in organic NLO materials, it is impossible to speed-up the developing of hybrid photonic platforms. On the other hand, the collaboration between materials and devices provides a stage to achieve the unprecedentedly high-performance organic NLO materials. This review will give a summary in the recent progress of organic second- and third-order NLO materials in Jen group. Particular emphasis will be addressed on how we remove the barrier for the application of second-order NLO materials in concise chromophore synthesis and thin-film engineering. And for third-order NLO materials, we will focus on introducing our recent advances of designing cyanines with large macroscopic NLO effects suitable for all optical signal processing (AOSP) applications. The applications and perspectives of advanced organic NLO materials are also discussed, which we believe that will inspire more close synergetic innovation from fundamental study in materials to photonic device engineering and then to overall system architecture.

2. Principle of nonlinear optics

Nonlinear optics is the science of the nonlinear relationship between the response of matter under intense light (laser) and the field strength. When light propagates in a medium, the valence electrons in the medium under the action of the photoelectric field produce a charge transfer relative to the atoms, causing the medium's polarization. The relationship between its polarization intensity and the photoelectric field intensity E of the incident light can be express as

$$p = \alpha E + \beta E^2 + \gamma E^3 + \ldots \quad (1\text{-}1)$$

or

$$P = \varepsilon_0 \chi^{(1)} E + \varepsilon_0 \chi^{(2)} E^2 + \varepsilon_0 \chi^{(3)} E^3 + \ldots \quad (1\text{-}2)$$

In equation 1-1, p is the polarization intensity of a microscopic molecule under an applied electric field and α, β and γ are the linear polarizability, the first-order hyperpolarizability and the second-order hyperpolarizability. The term of β denotes the second-order NLO coefficient of the molecule and γ denotes the third-order NLO coefficient. In equation 1-2, P is the macroscopic polarization strength of the material, ε_0 is the vacuum dielectric constant, $\chi^{(1)}$ is the first-order (linear) polarization rate, $\chi^{(2)}$ is the second-order nonlinear polarizability, $\chi^{(3)}$ is the third-order nonlinear polarizability, and so on.

In the case of a weak electric field, the high-order terms of equations 1-1 and 1-2 can be neglected from the second term onwards. Therefore, the polarization and the electric field strength E are linearly related, which belongs to the category of linear optics. When under laser action, the optical field is stronger, and the high-order terms from 2nd to nth in equations 1-1 and their corresponding terms in equation 1-2 cannot be ignored. So the microscopic polarization p and macroscopic P of the medium are not linearly related to the strength of the applied electric field E, which is the NLO effect. The effect associated with the 2nd term is called second-order NLO effect, referred as "microscopic second-order polarizability (β)" at the molecular level and as "macroscopic second-order susceptibility ($\chi^{(2)}$)" on the materials level. For second-order NLO materials, macroscopic second-order susceptibility is described by the following equation:

$$\chi^{(2)} = Nf(\omega)\beta_{ijk} < \cos^3\theta > = {Nf(\omega)\beta_{ijk}\mu E_p}/{5kT} \quad (1\text{-}3)$$

where N is the number of dipolar molecule, $f(\omega)$ is the Lorenz-Onsager local field factor, β is the hyperpolarizability of dipolar molecule, μ is the dipole moment, E_p is the poling electric field, k is the Boltzmann constant and T is the temperature. The dipole moment μ interacting with a poling field of E_p, competes with thermal randomization to define dipolar order $<cos^3\vartheta>$. For organic second-order NLO materials, the product $\mu\beta$ is often referred to microscopic molecular Figure-of-merit for push-pull chromophores. For a film poled in the z-axis, the macroscopic nonlinearity is r_{33}, which is also named Pockels effect or electro-optic (EO) effect, and the product $n^3 r_{33}$ is referred to the macroscopic Figure of merit. A typical application of organic EO materials is the electro-optic modulator for phase or intensity modulation. The input light is launched into the first Y branch of Mach-Zehnder interferometer (**Fig. 1a**), which is divided into two paths and transmitted along the two arms with different widths, respectively, and finally combine in the second Y branch to produce interference. The electric-field is applied by the coplanar electrode to induce the refractive index change of two arms (EO polymers) by Pockels effect, resulting in a significant changes in phase difference between two arms and hence a palpable drift in the output spectrum. So the electric signal can be used to modulate the optical signal.

This journal is © The Royal Society of Chemistry 20xx

Please do not adjust margins

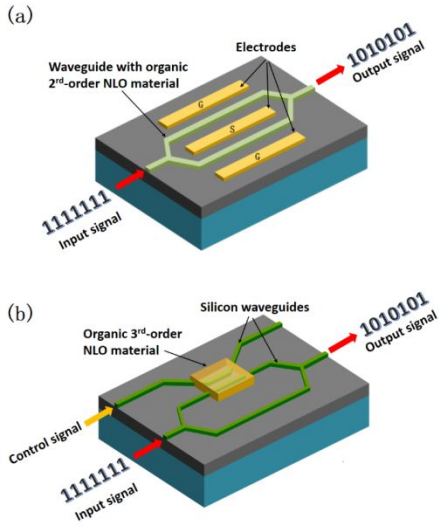

Fig. 1 (a) Illustration of EO modulation in polymer Mach-Zehnder interferometer waveguide with coplanar electrodes; (b) Illustration of AOSP using a Mach–Zehnder configuration in a silicon–organic hybrid device. **Fig. 1b** is modified from Ref. 56. Copyright, 2014, American Chemical Society.

The effect correlated to the third-order of electric field (E^3) is third-order NLO effect, which is referred as "microscopic third-order polarizability (γ)" at the molecular level and as "macroscopic third-order susceptibility ($\chi^{(3)}$)" on the materials level. Based on the sum-over-states (SOS) approach, γ can be simply described by the following equation,[54]

$$\gamma \approx \frac{\mu_{ge}^2 . \Delta\mu_{ge}^2}{\left(E_{ge} - \hbar\omega - i\Gamma\right)^2 \left(E_{ge} - 2\hbar\omega - i\Gamma\right)} \quad (D\ term)$$

$$+ \sum_{e'} \frac{\mu_{ge}^2 . \mu_{ee'}^2}{\left(E_{ge} - \hbar\omega - i\Gamma\right)^2 \left(E_{ge'} - 2\hbar\omega - i\Gamma\right)} \quad (T\ term)$$

$$- \frac{\mu_{ge}^4}{\left(E_{ge} - \hbar\omega - i\Gamma\right)^2 \left(E_{ge} + \hbar\omega - i\Gamma\right)} \quad (N\ term) \qquad (1\text{-}4)$$

where μ, $\Delta\mu$ and E represent the transition dipole moments, the difference in state dipole moments, and the transition energies, respectively, $\hbar\omega$ is the photon energy, Γ is the damping factor, while g, e, and e' subscripts denote the ground, first excited, and higher-lying excited states, respectively. As seen, three terms have been included in this equation, known as D for the dipolar term, T for the two-photon term and N for the negative term, respectively. Since D and T terms contains two-photon resonances ($2\hbar\omega$) in their denominators, both of them are directly related to the process of two photon absorption (TPA), and referred to as the imaginary component of γ, i. e. (Im(γ)). On the other hand, N term belongs to the real component of γ, i. e. (Re(γ)), which is proportional to the nonlinear refractive index that describes the change of refractive index under high intensity light irradiance. Re(γ) can be positive or negative, and in general the larger |Re(γ)| means a more pronounced change of the material index will be generated upon increasing the light intensity; this attractive feature therefore can be used for a variety of optical switching applications such as AOSP.[55] **Fig. 1b** shows a typical Mach–Zehnder device structure for AOSP.[56] In this device, the output signal will be similar to the incoming one without an external perturbing control light. However when an control light is applied, the refractive index of the NLO material will be modulated substantially to enable a clear optical phase change of signal light passing through the NLO material, thereby producing a new output signal.

3. Organic second-order NLO materials

The ideal EO materials for photonic device applications need to possess large Pockels coefficients (macroscopic r_{33} value), broad bandwidth capacity, high optical power handling, excellent processability, low dielectric constant, and low dielectric loss tangent, all simultaneously. The past two decades of vigorous research and development has gained very significantly at the fundamental understanding of organic EO materials' structure-property relationship.[57, 58] In the recent five years, we have been focused on the concise synthesis of high-performance polyene-based chromophores and self-assembled dendrimers. Considerable efforts have been made on the efficient poling of EO polymer films by nano-doping, wafer-scale poling on soda-lime glass substrate and exploitation of transparent graphene electrode for cladding-free poling. These research efforts are expected to remove the barrier to real application and to meet these specifications for photonic applications of high-performance organic EO materials.

3.1 Concise synthesis of highly efficient dipolar chromophores

Design and synthesis of donor-bridge-acceptor (D-π-A) chromophores exhibiting large molecular hyperpolarizabilities is one of the central themes in the research of highly efficient organic NLO materials for photonic applications.[59-63] Over the past two decades, extensive investigation of structure-property relationship for these highly NLO-active dipolar chromophores have significantly contributed to the understanding of their optical nonlinearity at the molecular level. Meanwhile, it also provided feedstock of organic EO materials enabling the development of advanced EO devices for optical modulation. Among those dipolar chromophores, push-pull tetraene chromophores containing strong CF_3-TCF acceptor are the best performing for NLO applications.[21, 24, 27] The conventional synthetic strategy of tetraene chromophores is step-wise forward synthesis (**Fig. 2a**), which is complicated and often gives low overall yields from multiple step reactions with considerable efforts in purification.[64-66] Moreover, as shown in **Fig. 3a**, the critical steps in the synthesis of NLO chromophores include the cryogenic lithiation and/or metal hydride reduction.[67] These reaction protocols clearly demand well-trained synthetic chemists with special know-how and experience, and specific apparatus and equipment for both lab synthesis and scale-up production, posing limitation and operational cost in scale-up synthesis.

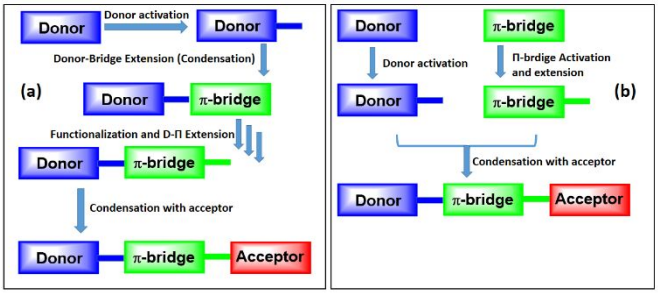

Fig. 2 (A) Step-wise forward synthesis of dipolar NLO chromophores; (B) Convergence and MCR are the keys to high synthetic efficacy to overcome the current limitation of step-wise routes. D: electron-donor; π: conjugated bridge; A: electron-acceptor.

Inspired by recent surge of interest in multicomponent reactions (MCRs), the synthesis of push-pull polymethine chromophores was designed and optimized *via* new protocols of three component reaction (3-CR) by mixing the donor, conjugated bridge and acceptor in one pot (**Fig. 2b**).[68, 69] The use of highly reactive bisaldehydes is the key to improve the synthetic efficacy of heptamethine merocyanines over that of dipolar polyenes. As shown in **Fig. 3b**, the high chemo-selectivity of bisaldehydes and their relative condensation reaction rates with both basic and acidic active methylene compounds drive a predominate formation of asymmetric dipolar structures under the 3-CR conditions. In comparison with sequential multistep synthesis, the 3-CR conditions is concise and without the use of pyrophoric organo-lithium reagents. In electro-optics, very large EO coefficients up to 150 pm/V at 1.3 μm have been obtained in poled polymers (chromophore loading density 33%), which is very comparable to that of a push-pull tetraene chromophore containing CF_3-TCF (2-(3-cyano-5-methyl-5-(trifluoromethyl)furan-2(5H)-ylidene)malononitrile) acceptor. This new efforts may fulfil the critical transition from lab to the scale-up synthesis of highly efficient NLO chromophores for EO polymers. Further investigation can be emphasized on more in-depth analysis of structure-property relationships and structure modification on the electron-bridge, where the chloride on bridge provides an active site for introduction sit-isolating groups.

Molecular glass is one of the most attractive chromophores due to its high chromophore loading density, enabling high refractive index and large macroscopic r_{33} value in poled film.[14, 70] Through intermolecular interactions such as hydrogen-bonding, π-π stacking, or Van Der Waals interaction, neat chromophores can self-assemble into monolithic molecular glass films. The first demonstration of EO molecular glass was based on the π-π stacking self-assembly (ArH-ArF interactions) of dendritic phenyl on donor and dendritic pentafluoro-phenyl on bridge.[71] Then series of polyene-based molecular glasses with dendritic aryl (phenyl, naphthyl and anthracyl) and pentafluoro-phenyl were synthesized to tune the self-assembly to realize the ultra-large r_{33} value of up to 318 pm/V @ 1310 nm, as shown in **Fig. 4a**.[72] Their self-assembly is driven by the enhanced cohesive energy of heterodimers, the schematic illustration of which is shown in **Fig. 5a**. Notably, the self-assembled molecular glass based on heterodimers requires two different dendritic groups. In association with the complicated protocol of tetraene chromophore (**Fig. 4a**), the synthetic efforts of such molecular glass with heterodimerization are time-consuming and low-efficiency in comparison with those chromophores for guest-host doping.

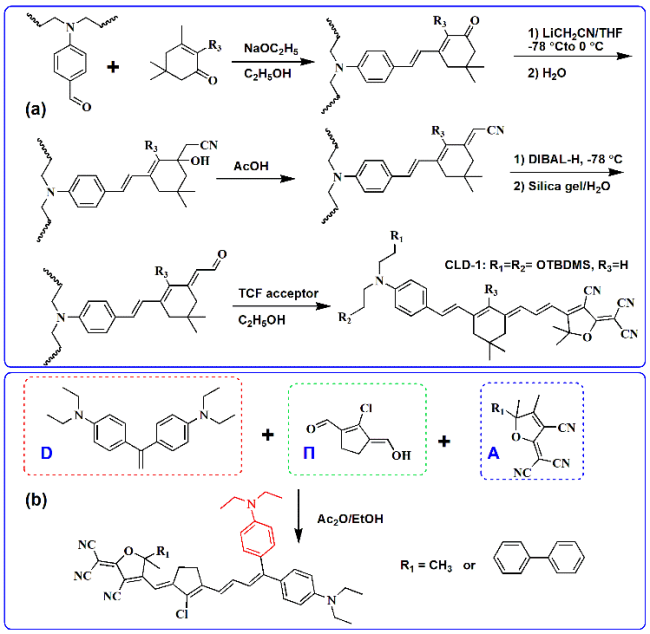

Fig. 3 The traditional step-wise forward synthesis (a) and the three-component modified concise synthesis (b) of tetraene-based chromophores.

This journal is © The Royal Society of Chemistry 20xx

Please do not adjust margins

ARTICLE

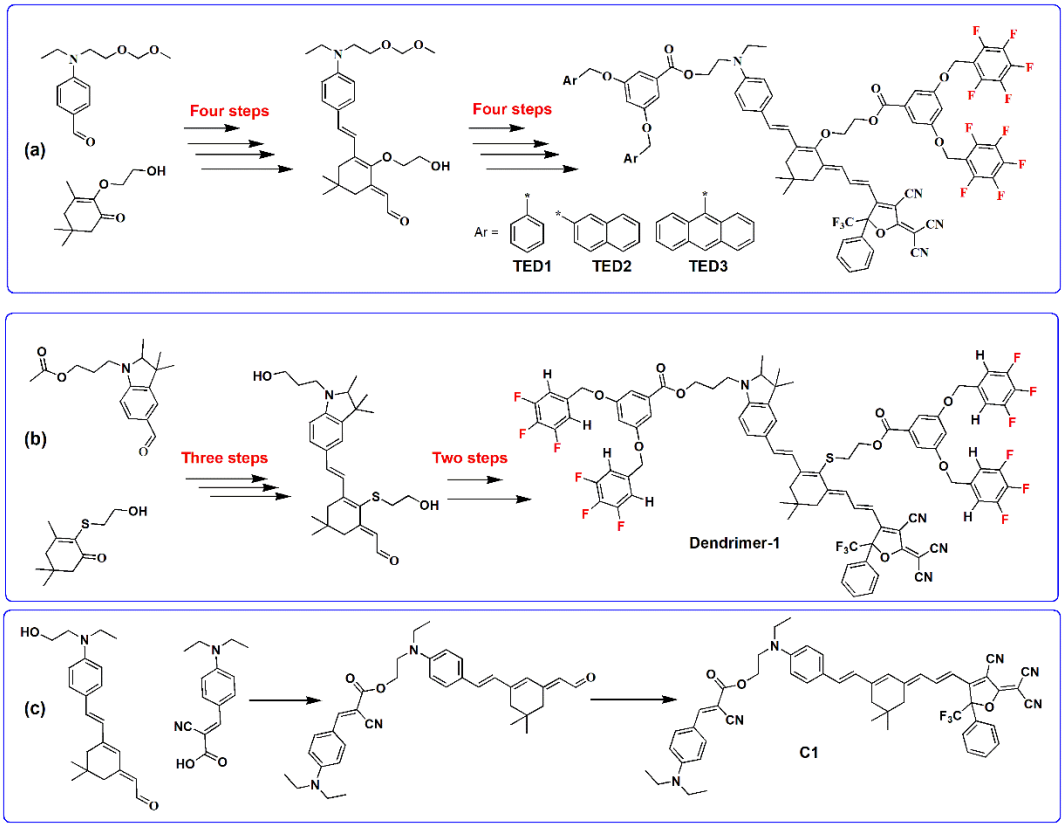

Fig. 4 Synthesis of tetraene chromophores with different self-assembled dendrons (a) and with same dendrons (b); (c) synthesis of tethered binary NLO chromophores.

Very recently, we developed a new self-assembly strategy of supramolecular homodimerization to self-assemble EO dendritic films, in which two dendritic units with semifluorinated dipolar 1, 2, 3-trifluorobenzene (TFB) moieties were attached to the donor end and the π-bridge of push-pull tetraene chromophores.[73, 74] In these new dendrimers, the use of monolithic and semifluorinated TFB rings was to replace the heterodimers of phenyl and pentafluorophenyl moieties. As shown in **Fig. 4b**, it greatly simplified the synthesis of EO dendrimers and their thin-film processing. The semifluorinated TFB contains a dipole moment of 3.0 D, prone to form antiparallel packing due to dipole-dipole interaction. Unlike ArH-ArF heterodimerization, the self-assembly between TFBs is homogeneous (**Fig. 5b**). The poled films of these self-assembled dendritic EO films showed very large EO coefficients up to 248 pm/V at the wavelength of 1310 nm, and excellent temporal stability at room temperature with a very minimal change of ~5% for over 1000 hours. Our study therefore illustrated that homodimer stacking of TFB rings through the dipole-dipole stacking gives stabilization energy similar to that of quadrupolar interaction of phenyl and pentafluorophenyl heterodimeric pairs. More significantly, the poling efficiency (r_{33}/E_p, **Fig. 6**; E_p: poling electric-field) of TFB-containing self-assembled EO dendrimers was much higher than ArH-ArF self-assembled dendrimers (TED 1-3) and guest-host films, due to highly dipolar dielectric environment with dipolar TFB dendrons. Therefore, the efficiency in synthesis and poling are both improved, paving the way for the application of self-assembled chromophores in photonic devices.

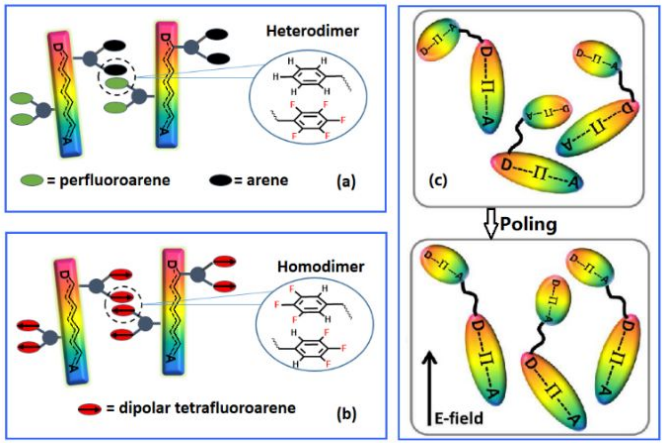

Fig. 5 Schematically illustration of heterodimerization (a) and homodimerization (b) self-assembly of molecular glass and the poling process of tethered binary chromophores (c). Reproduced from Ref. 74 and 75 with permission from the Royal Society of Chemistry.

A new molecular glass design of tethered binary chromophores has been studied for electro-optics. As shown in **Fig. 4c**, a push-pull tetraene structure with strong dialkylaminophenyl donor and CF_3-TCF acceptor is used as the primary chromophore due to its large hyperpolarizability. And a short cyanoacetate dye with relatively smaller dipole moment and very different molecular aspect ratio is used as a secondary dipolar structure for dipole engineering.[75] We found that such binary chromophore systems (exemplified as chromophore C1) exhibited significantly improved poling efficiency and thermal stability in poled films of guest-host polymer and monolithic glass. The introduction of secondary dipolar cyanoacetate dye (dipole moment: ~5D) significantly attenuated the dipole-dipole electrostatic interactions and prevented close packing between the primary dipolar structures (illustrated in **Fig. 5c**). Ultrahigh r_{33} value of 273 pm/V and high refractive index of 2.12 at the wavelength of 1300 nm have been achieved from monolithic glass of C1, which represented a record-high n_3r_{33} Figure-of-merit of 2601 pm/V with good temporal stability. This exceptional result is a great demonstration of the advantages offered by dynamically assisted dipolar polarization enhancement of tethered binary chromophores, for significantly improving the poling efficiency and thermal stability of organic EO materials for efficient optical modulation.

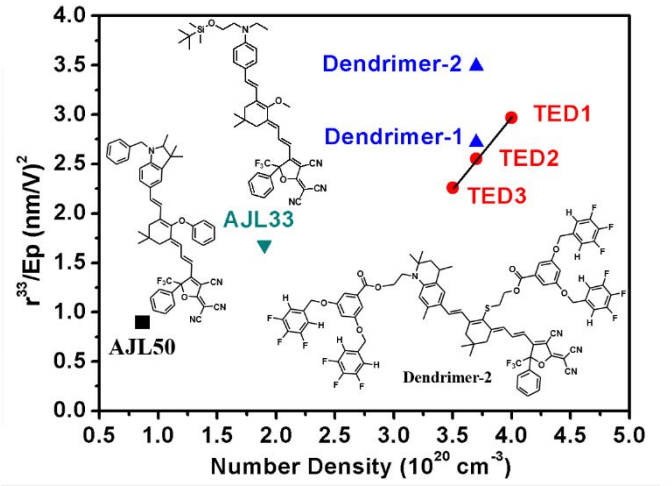

Fig. 6 Comparison of poling efficiency of EO molecular glass and guest-host EO polymer. AJL50: 13 wt% chromophore in PMMA; AJL33: 25 wt% chromophore in PMMA. Reproduced from Ref. 74 with permission from the Royal Society of Chemistry.

3.2 Efficient poling of EO polymer films for optical waveguides

The noncentrosymmetric order of dipolar chromophores through electric-field poling is the critical initial step in processing EO polymer films for their application in optical waveguides. The most commonly used poling is contact poling, which has been used in various electro-optic devices such as SOH, POH and all-polymer EO waveguide. However, contact poling still suffers from thin film dielectric breakdown due to current injection from metal electrode. Therefore, achieving large-area and efficient poling is still a challenge. In addition, the high optical absorption losses of metal electrodes greatly limit the waveguide fabrication and poling efficiency, which is also a problematic issue for electro-optic polymer applications. Although the use of BCB dielectric protective layers, pyroelectric poling, and sol-gel highly conductive cladding have been reported to solve the poling difficulty, high-efficiency electric field poling still remains an important challenge that needs to be addressed.[76-84] Recently, we have investigated the regulation of the dielectric constant by nano-doping, preparation and large-area poling of EO polymer on soda-lime glasses, as well as the development of low-optical-loss graphene electrode to replace metal electrodes for electric field poling. These efforts are expected to facilitate the efficient poling of EO polymers in waveguide devices for a wide range of applications.

This journal is © The Royal Society of Chemistry 20xx

Please do not adjust margins

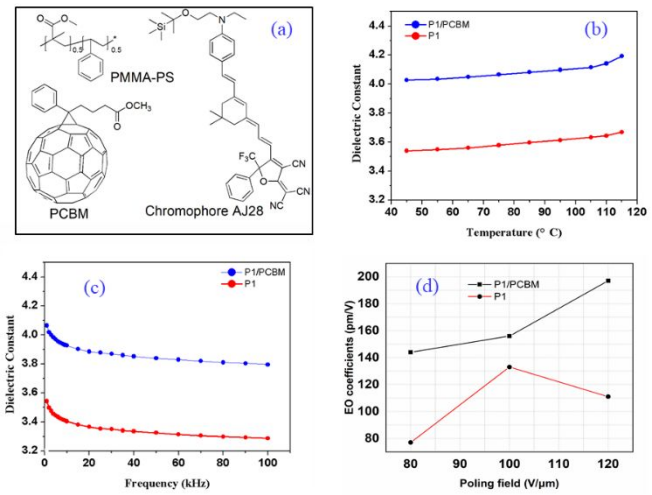

Fig. 7 (a) Chemical structures of fullerene PCBM, guest chromophore AJ28 and host polymer PMMA-PS; (b) temperature-dependent dielectric constant of EO films; (c) dielectric constant of EO films at frequency from 1 kHz to 100 kHz; (d) EO coefficients under different poling electric-field. P1/PCBM: 20wt% AJ28 and 5% PCBM in PMMA-PS; P1: 20wt% AJ28 in PMMA-PS. Reproduced from Ref. 86 with permission from the Royal Society of Chemistry.

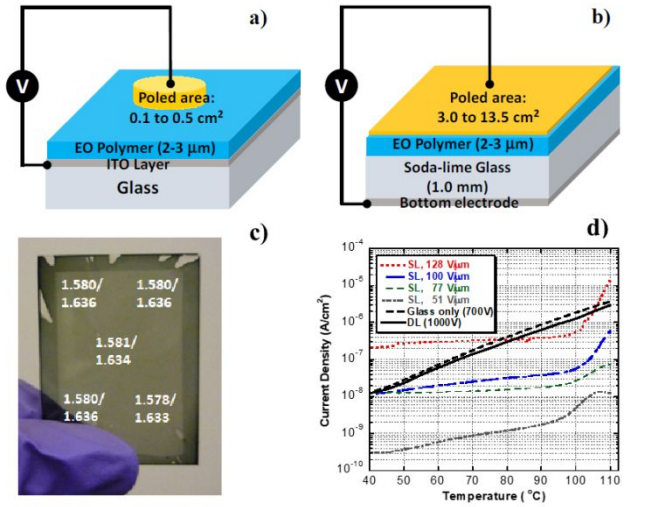

Fig. 8 (a) Standard poling of a single layer EO polymer film sandwiched between two electrodes; (b) Large-area poling design of this study using a double-layer stack consisting of a μm-thick EO thin film and a millimeter-thick soda-lime glass substrate sandwiched between ITO electrode and gold electrode (marked in yellow); (c) the photography of large area (13.5 cm^2) EO film on soda-lime glass; (d) Current density versus temperature plots for different poled samples of AJLZ53/PMMA-PS(SL: single layer, Fig. 8a; DL: double layer, Fig. 8b). The current profile of Corning's soda-lime glass (1.0-mm thick) was provided for comparison. Reproduced from Ref. 87 from Optical Society of America.

The high electron affinity, electron mobility and percolated networks for electron transport of fullerene derivatives, such as PCBM, have established them as excellent electron acceptors and transport materials in organic solar cells and electronic devices.[85] In this work, PCBM was doped into the EO polymers to regulate the dielectric constant of EO films (**Fig. 7a**).[86] It was found that dielectric constant was significantly increased from 3.54 (P1) to 4.02 (P1/PCBM) as well as the refractive index increase from 1.6335 to 1.6554. Temperature-dependent dielectric constant measurements (**Fig. 7b** and **7c**) revealed that, at the poling temperature, dipole moment of AJ28 in P1/PCBM was significantly increased to three-fold original dipole moment at room temperature. This enhanced dipole and polarizable environment of chromophores in P1/PCBM resulted in the significant improvement of poling efficiency, as shown in **Fig. 7d**. Larger EO coefficients (197 pm/V versus 133 pm/V) and Figure-of-merit n^3r_{33} (1002.9 pm/V versus 632.2 pm/V), as well as higher order parameter (15.7% versus 10.6%) and birefringence were achieved in PCBM-doped film P1/PCBM. Those results revealed how the microscopic environment change of chromophore influenced the macroscopic EO activities, demonstrating the significant application potential of fullerene in organic EO materials and devices for efficient poling.

Efficient poling of high performance electro-optic (EO) polymer thin films at the wafer scale (>10 cm^2) is a key step towards the realization of integrated photonic systems capitalizing on significant performance improvement of these materials.[61] However, in common poling protocols of EO polymers, the poled areas are mostly limited to the range of 0.10×0.50 cm^2 (**Fig. 8a**) in order to obtain consistent results of poled thin film samples in good yields. It remains a great challenge for researchers to further increase the effective poled area. In this work, we demonstrated a simple protocol for repeatable and efficient contact poling of guest-host EO polymer thin films over large areas on soda-lime glass substrates (**Fig. 8b** and **8c**).[87] At temperatures close to T_g, the leak-through current of single-layer films showed the characteristic spike under high poling fields just prior to dielectric breakdown of the polymer film, as shown in **Fig. 8d**. In contrast, the poled film on soda-lime (DL) gave a steady pseudo-linear increase of leak-through current (LTC) from 40 °C to 110 °C and no current spikes were observed. The poled large-area (**Fig. 8c**, up to 13.5 cm^2, the largest poled film, to the best of our knowledgement) thin films exhibited very large second-order nonlinear susceptibilities (d_{33} values of 330-520 pm/V) for second-harmonic generation (SHG) and associated large Pockels coefficients (r_{33} values of 105-180 pm/V) at the wavelength of 1.3 μm, as listed in **Table 1**. The order parameter of poled film on soda-lime glass was quite comparable to that of conventional SL films. The poling protocol also produced poled EO thin films with excellent optical homogeneity and large positive birefringence with small variation (~10^{-3}) of refractive indices over the poled large areas. Since it is very easy to fabricate waveguide by ion exchange of soda-lime glass, this study suggests a viable and scalable path towards the

realization of integrated photonics based on pre-poled thin films of high performance EO polymers.

Table 1. Poling results of EO polymer ALZ53/PMMA-PS

Sample Entry	Configuration, Poled area	Poling field (V/μm)	r_{33} at 1.3 μm (pm/V)	n_{TE}/n_{TM} at 1.3 μm	Order parameter
1	-	-	0	1.592/1.590	-
2	SL[a], 0.5 cm²	51	50	1.590/1.602	4.0%
3	SL, 0.5 cm²	77	74	1.586/1.615	9.4%
4	SL, 0.5 cm²	100	101	1.583/1.632	15.4%
5	SL, 0.5 cm²	128	125	1.580/1.653	21.9%
6	DL[b], 3.2 cm²	115	110[c]	1.581/1.642	18.8%
7	DL, 13.5 cm²	110	105[c]	1.581/1.636	17.2%

[a]SL: single-layer EO thin films, corresponding to the configuration shown in Fig. 8a; [b]DL: double layer containing EO thin film and soda-lime glass substrate, corresponding to the configuration shown in Fig. 8b; [c]r_{33} values are extrapolated from the order parameters of poled samples.

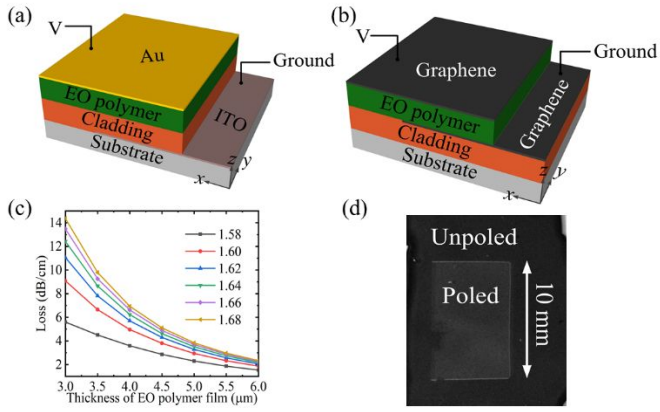

Fig. 9 Schematic diagrams of EO polymer slab waveguides with (a) conventional Au/ITO electrodes and (b) graphene electrodes, where light propagates in the y direction; (c) transmission loss of slab waveguide as a function of thickness of EO polymer film, which is sandwiched by top and bottom graphene electrodes (as shown in b, $n_{cladding}$ = 1.573); (d) photography of poled sample using transparent graphene electrode. The EO polymer used in this study is a simple guest-host system by doping 15 wt% of dipolar polyene chromophore AJLZ53 into PMMA-PS. Reproduced from Ref. 88 from Optical Society of America.

In terms of optical loss, most of poled second-order NLO polymer films shows measured transmission loss of 1 to 2 dB/cm. Such optical loss is routine for all-polymer EO devices. For compact silicon waveguide with high refractive index contrast between EO material and silicon, the device footprints are in the ranges of several millimeter. Therefore, the transmission loss ascribed to EO material is less than 1 dB. For more compact plasmonic waveguide, the length of electro-optic modulation is always less than 1 millimeter, in which the EO material induced optical loss is negligible. However, metal and indium tin oxide (ITO) electrodes used in electric poling are of high loss. To reduce the electrode-induced optical loss, there should be a thick buffer layer placed between bottom metal or ITO electrode and the EO film. The presence of the buffer layer, however, increases the poling voltage. The choice of a buffer material that has both high conductivity and good optical transparency is a challenge. To address this issue, we have develop the monolayer graphene as the poling electrode for electric-field poling of EO polymer films.[88] Two kinds of EO polymer slab waveguide were fabricated. In the reference samples S1 and S2 (**Fig. 9a**), the EO polymer films were sandwiched between ITO and gold (Au) electrodes with buffer layer epoxy resin. For the other samples S3 and S4 (**Fig. 9b**), the EO polymer films were sandwiched between two graphene electrodes without any buffer layers so that the EO polymer films were in direct contact with the graphene electrodes. We calculated the graphene-induced losses of the TM mode, where the monolayer graphene electrodes were modeled as conductive boundaries with a complex conductivity of 6.084×10^{-5} - $j7.519\times10^{-6}$ at 1550 nm. As shown in **Fig. 9c**, the graphene-induced loss was highly related to the thickness and refractive index of the EO film, which was explained by the fact that a stronger light confinement in the EO polymer film with a thicker film or with larger refractive index leads to a weaker mode field at the graphene electrodes and hence a smaller graphene-induced loss. Theoretically, the graphene-induced optical loss can be as low as 1 dB/cm for each single-layer graphene electrode. Our results also showed that poling with graphene electrodes did not introduce significant additional optical loss to the EO polymer. The poling results are listed in **Table 2**. We have achieved high EO coefficients of 82 pm/V at 1541 nm and 110 pm/V at 1300 nm with a poling voltage of only 420 V, which was much lower than that required by using traditional metal electrodes. The use of graphene electrodes for poling allows the use of inexpensive cladding material and more flexible waveguide designs. The upper graphene electrode can be further patterned to form low-loss modulation electrodes for the EO device to be made. Such a graphene/EO polymer hybrid platform can be explored as a key solution to overcome the traditional tradeoff between poling efficiency and optical loss. Meanwhile, it significantly simplify the design and fabrication of waveguide devices based on EO polymer.

Table 2. Summary of poling results for Sample S1, S2, S3, and S4

	Poling field	n_{TE}/n_{TM} @1300 nm	n_{TE}/n_{TM} @1541 nm	r_{33} @1.3 μm/pmV^{-1}	r_{33} @1.5 μm/pmV^{-1}
S1	910 V	1.592/1.621	1.577/1.598	70	33
S2	800 V	1.588/1.638	1.574/1.610	100	67
S3	350 V	1.586/1.628	1.573/1.604	91	54
S4	420 V	1.585/1.646	1.573/1.617	110	82

Configuration of slab waveguides S1 and S2: **Fig. 9a**; S3 and S4: **Fig. 9b**.

This journal is © The Royal Society of Chemistry 20xx

Please do not adjust margins

3.3 Application of EO polymer: unprecedented high-performance EO modulation

For developing a range of prospective applications, optical modulators need to have high modulation speeds, large bandwidths and small footprints, low losses, and ultralow power consumption. However, these requirements often contradict each another in silicon-based or III-V semiconductor modulators. Our high performance EO polymers can be considered as a sufficiently viable technological solution, and also become very competitive with semiconductor materials. The rapid progress of EO material has pushed forward many significant advances in the development of high-speed and broadband information technologies.

Table 3. The state-of-the-art SOH, POH, Sol-gel/polymer and all-polymer EO waveguides with organic EO materials SEO125 or SEO100 (2017 to present)

Device type	Device configuration	Device performance	EO material	EO coefficients in device
SOH quantum microwave-to-optical transducer	Photonic crystal reflector	Electro-optic coupling rate: 590 Hz at 7 mK; bandwidth: 20.3 MHz	SEO100	106 pm/V
POH EO modulator	Mach-Zehnder interferometer	3-dB bandwidth > 360 GHz (0.36 THz)	SEO100	64 pm/V
SOH EO modulator	MZI slot waveguide	line rates of up to 120 Gbit/s; V_p = 0.9 V	SEO100	146 pm/V
SOH EO modulator	Sub-wavelength grating waveguide ring resonator	3-dB bandwidth > 40GHz; power consumption: 2.6 fj/bit;	SEO125	54.7 pm/V
SOH EO modulator	One-dimensional photonic crystal slot	V_pL= 1 V · cm; bandwidth = 61 GHz;	SEO125	490 pm/V (with slow-light effect)
Sol-gel/Polymer hybrid EO modulator	Mach-Zehnder interferometer	3-dB bandwidth: 120 GHz; V_pL =1.8 V cm	SEO100	160 pm/V
All-polymer millimeter-wave EO phase modulator	Channel waveguide with in-plane slotted patch antennas	Modulation index: 0.03 rad (RF power density of 15 W/m^2); Figure-of-merit: 1.1 W$^{-1/2}$	SEO125	50 pm/V
Surface-normal plasmonic EO modulator for free space communication	Sub-wavelength metal grating	V_p =20 V @ 1KHz	15wt%AJLZ53 in PMPS	60 pm/V @ 1522 nm

Electro-optic polymers have been widely used in different types of photonic devices such as POH, SOH, Sol-gel/polymer hybrid and all-polymer EO modulators. **Table 3** lists the state-of-the-art EO modulation with EO polymer SEO125 or SEO100 provided by our group in the past three years. Low-loss fiber-optic links have the potential to connect superconducting quantum processors together over long distances to form large scale quantum networks. A key component of these future networks is a quantum transducer that coherently and bidirectionally converts photons from microwave frequencies to optical frequencies. In 2016, we verified the EO properties at 7 K of poled guest-host EO polymers consisting of AJLZ53 chromophores for the first time, indicating the potential of EO polymer for photonic devices for quantum communication.[89] In 2020, our collaborators from Stanford University presented a platform for electro-optic photon conversion based on silicon-organic hybrid devices with SEO100.[90] This EO device combined high quality factor microwave and optical resonators with an electro-optic polymer cladding to perform microwave-to-optical photon conversion from 6.7 GHz to 193 THz (1558 nm). The device achieved an electro-optic coupling rate of 590 Hz in a milliKelvin (7 mK) dilution refrigerator environment. Electro-optic polymers have a low dielectric constant and thus allow for excellent speed matching of light waves and RF signal. Our collaborators from Karlsruhe Institute of Technology used SEO100 to fabricate plasmonic waveguide EO modulator, enabling high-speed electro-optic modulation with record-breaking bandwidth up to 360 GHz with the phase shifter length of 20 μm and a proof-of-concept demonstration of 16-meter-long terahertz communication has been reported.[27] In the SOH EO modulator filled with SEO100 in slot, the line rates of up to 120 Gbit/s and V_p of less than 1 V was achieved.[91, 92] In waveguide micro-ring resonator with sub-wavelength grating structures, the use of SEO125 as a cladding results in energy consumption as low as 2.6 fj/bit.[93, 94] In SOH EO modulator using the SEO125 material in combination with the One-dimensional photonic crystal and slot structure, we have achieved a bandwidth of up to 61 GHz and an in-device EO of 490 pm/V.[33, 95] Meanwhile, there have been significant advances in the bandwidth optimization of Sol-gel/polymer hybrid devices, and bandwidths up to 120 GHz have been achieved with V_pL as low as 1.8 V cm.[96] In all-polymer devices, the scientists from University of Maryland used SEO125 to realize the millimetre-wave phase modulation with high Figure-of-merit and RF power density of 15 W/m.[2,97] Besides on-chip modulation, recently, Ren et al. demonstrated a surface-normal plasmonic modulator using sub-wavelength metal grating.[98] The device consists of a 1.77 mu m efficiently poled electro-optic polymer film, which is sandwiched between a plasmonic grating and an indium-tin oxide film. A strong Fano resonance with a sharp plasmonic bandgap at 1522 nm wavelength was observed and electro-optical modulation was demonstrated with Vp of 20 V for three dimensional optical interconnects.

In general, those applications of EO materials in different type of hybrid waveguides significantly solved the problems of energy consumption, rate and bandwidth in electro-optic modulation. Successful deployment of these EO polymer-based materials and subsystems will significantly contribute to a broad spectrum of photonic technologies for applications, including the systems such as fiber optic networks for future internet infrastructures, board-band and chip-level optical interconnects for next generation supercomputers in smart data centers and enterprise networks, light-weight high bandwidth optical links for intra-aircraft communications, quantum communication, terahertz imaging/sensing, optical synthesizers, nonintrusive electric-field sensors, beam-steering in phased array radar and antennas, sensors *etc*.

4. Organic third-order nonlinear materials

4.1 Cyanine-based AOSP materials

For third-order nonlinear optics, design guideline and optimal structure of active chromophores is quite different from those for second-order nonlinear optics. Typically, chromophores for third-order NLO consist of symmetric structures of donor-bridge-donor (D-π-D) or acceptor-bridge-acceptor (A-π-A). For the application in AOSP at the wavelength of interest, the used third-order NLO materials should not only have large nonlinear optical coefficients, but also exhibits very low optical losses including both linear and nonlinear loss. Typically, for transparent materials, the NLO loss mainly arises from TPA. As a result, it is quite useful to define a TPA Figure-of-merit (FOM) for AOSP materials, which is denoted as |Re(γ)/(Im(γ)| at the molecular level, while as $|\mathrm{Re}\chi^{(3)}/\mathrm{Im}\chi^{(3)}|$ in bulk materials level. In general, the material FOM value needs to be beyond 12 to ensure a feasible AOSP.[55, 99] Silicon is one of attractive candidate materials for AOSP applications due to its ability of guiding light at nanoscale and ease of chip-scale photonic integration, its third-order NLO response, however, is limited by the deleterious TPA and long-lived free carrier effects, thereby leading to poor material FOMs.[55] Thus, numerous efforts have been devoted to exploring new organic materials with extensive π-system for AOSP applications, among which interest in using symmetrical cyanine dyes has increased more rapidly due to their very excellent molecular third-order NLO effects achieved at optical telecommunication wavelengths (1300 nm and 1550 nm).[50, 56] For example, shown in **Fig. 10a** is the structure of a representative selenopyrylium-based cyanine dye (Se-7C) reported by Prof. Marder and Prof. Perry et al. in 2010, which, at 1550 nm, can not only demonstrate a quite large Re(γ) value of 2×10^{-31} esu, but also an unprecedentedly high molecular FOM up to 190.[100]

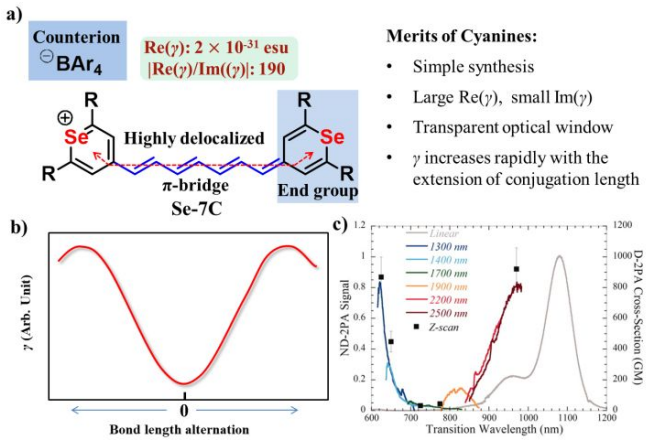

Fig. 10 a) Chemical structure of a representative selenopyrylium-based cyanine (Se-7C) with Re(γ) and |Re(γ)/(Im(γ)| values noted (left), and illustration of cyanine merits (right); b) Variation of polarization γ plotted versus BLA for a simple donor–acceptor polyene. c) Nondegenerate 2PA spectra of **Se-7C** solution under different pump wavelengths. **Fig. 10c** is adopted from Ref. 91. Copyright, 2010, American Association for the Advancement of Science.

Cyanine dyes are an intriguing class of ionic π-conjugated organic molecules having an odd-number of sp^2-hybridized carbon atoms in the polymethine-based conjugated bridge.[101] In general, the charge of symmetrical cyanines is highly delocalized over the conjugated bridge, making the bond-length alternation (BLA) between the adjacent C-C bonds almost close to zero, so-called "cyanine" limit. At this "cyanine" limit, the magnitude of Re(γ) can reach the maximal value according to the simplified SOS perturbation theory shown in **Fig. 10b**.[102] This is because the above structure feature of cyanines can endow them with a large transition dipole moment (μ_{ge}) and a small energy gap (E_{ge}) between the ground-state and first-excited state. In addition, symmetric cyanines not only exhibit a narrow electronic absorption band with sharp low energy band edge, but also a large energy spacing between the first (one-photon (1PA) allowed) and the second (two-photon (2PA) allowed) excited states, thereby giving rise to advantages of low linear and NLO absorption at the desired operational wavelengths.[100] Note that the energy of 2PA state is always about 1.7 times that of 1PA state. **Fig. 10c** shows the nondegenerate 2PA spectra of Se-7C in solution under different pump wavelengths, from which we can easily see a salient region where the 2PA is quite weak. Besides, another advantage of cyanines is their easily tunable structure by simply regulating the conjugation bridge, the terminated end-groups, and the counterions. Encouragingly, it has been well demonstrated that the magnitude of Re(γ) can be dramatically increased by extending conjugation length *L*, i.e. $\mathrm{Re}(\gamma) \propto L^n$.[103] For example, for selenopyrylium-based cyanines, upon increasing the conjugation length from 3C (three carbon atoms) to 5C (five carbon atoms), and to 7C (seven carbon atoms), the resulting |Re(γ)| can accordingly show an order of magnitude growth from 2.8×10^{-33} esu, to 2.3×10^{-32} esu, and to 2.2×10^{-31} esu.[100] Nonetheless, it is worth noting that if *L* is greater than C9 (nine carbon atoms), a Peierls-type symmetry breaking that localizes charge on one end of the molecule will often happen to cause the loss of the above-mentioned advantageous optical

This journal is © The Royal Society of Chemistry 20xx

Please do not adjust margins

properties of cyanines.[104-106] As a result, either how to maintain the symmetry of cyanines at long conjugation length beyond 9C or how to maximize the NLO effects as large as possible at a fixed conjugation length has been the interesting research topic in the field.

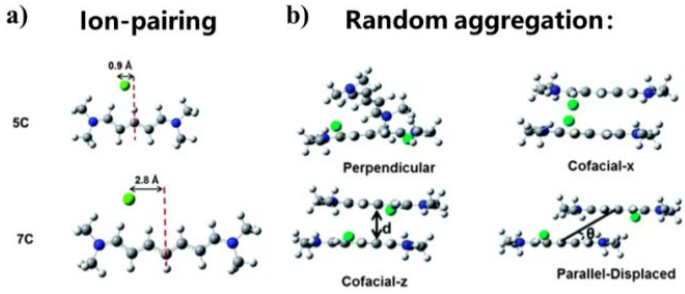

Fig. 11 Optimized ground-state structures (a) of monomeric streptocyanines (5C and 7C) and representations of the 5C aggregate dimers in the perpendicular, cofacial-x, cofacial-z, and parallel-displaced configurations (b) as determined at the uB97X-D/cc-pVDZ level of theory (carbons are represented in grey; hydrogens, white; nitrogens, blue; and chlorides, green).

To achieve the practical AOSP applications, these cyanine dyes have to be processable as high optical quality thin films with high loading chromophore density,[56] meaning that their excellent molecular γ of cyanines should be efficiently translated into the bulk $\chi^{(3)}$, which however remains a major challenge in the field. This is because cyanines are highly polarizable ionic molecules that are inevitably susceptible to strong chromophore-counterion (intramolecular) and chromophore-chromophore (intermolecular) interactions in the solid-state due to ion-paring or random aggregation (**Fig. 11**),[107, 108] which would lead to undesirable charge localization (charge of canines localizes towards one of terminated end groups or aggregates) to distort the favorable molecular symmetry of cyanines. Such symmetry breaking undoubtedly would increase the BLA and thus results in a dramatic reduction of $\chi^{(3)}$. Moreover, these strong intra- and intermolecular interactions can also enable a mixing of the excited state wave functions to shift and broaden both 1PA and 2PA bands, causing the loss of the originally excellent optical transparency window that significantly increases the linear absorption and TPA loss.[109, 110] To control and/or mitigate these adverse interactions, various molecular design strategies have been developed such as the use of bulky, soft counterions,[111] introduction of bulky, rigid spacers,[112-115] formation of polyelectrolyte-cyanine complexes, and so on.[116]

4.1 Design strategies of TCF-cyanines for AOSP applications

In the past decade, our research group has devoted significant efforts to studying anionic tricyanofuran (TCF)-terminated heptamethine dyes (**Fig. 12a**) for AOSP applications. TCF is a strong electron-withdrawing group widely used in second-order NLO field,[61] and as the terminal groups, the resulting anionic cyanines can display good solubility, intense and sharp NIR absorption centered at ~900 nm (**Fig. 12b**),[117] and respectable chemical/photochemical stability, comparable γ (>10^{-32} esu) to chalcogenopyrylium cyanines.[118] More importantly, we also were attracted by its another advantage, that is, TCF-cyanines, to some degree, is resistant to aggregation-induced effects based on the similarity between the solution and solid-state linear absorption spectra, attributed to the two steric methyl substituents in the TCF end-groups. However, when using the neutral polycarbonate (APC) as the host polymer to process high number density TCF-cyanine films, the resulting guest-host films always suffer from significant phase separation (**Fig. 12b**, insert), leading to undesirable scattering and absorption optical loss. To address this issue, we introduced tetraphenyl-substituted phosphonium-based cations with a somewhat delocalized positive charge to replace those traditional ammonium salts as the counterions for TCF-cyanines, which can not only reduce the ion-pairing effect, but also effectively improve the miscibility of cyanines and the host polymer.[118] As displayed in **Fig. 12c**, **AJBC1721** and **AJBC1722** -based 50 wt% doped guest-host films clearly show a phase-separation at a magnification of 100×, while the AJBC 1725 film remains optically homogeneous.

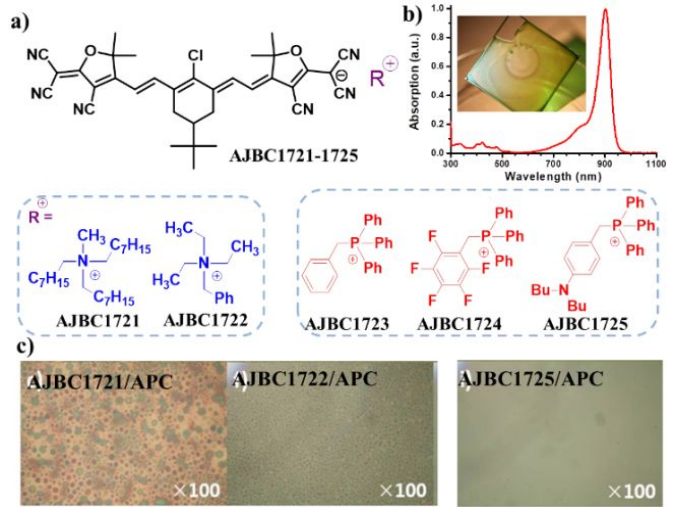

Fig. 12 a) Chemical structures of TCF-cyanines **AJBC1721-1725**; b) Linear absorption of **AJBC1721** in DCM solution (Insert: Photo of thick guest-host APC film doped with 50wt% of AJBC1721); c) Optical transmission micrographs of thick guest-host APC films doped with 50 wt% of different cyanines under 100 magnifications. **Fig. 12c** was adopted from Ref. 109. Copyright, 2012, John Wiley and Sons.

Third-order NLO properties of guest-host polymers of **AJBC1722-1725** were carefully studied through the femtosecond pulsed Z-scan method, which demonstrated that the effect of modulation of counterions on third-order NLO properties is small in both solution and film state with the magnitude of Re$\chi^{(3)}$ at about 3 × 10^{-11} esu at 1550 nm. However due to large TPA loss, a sub-optimal bulk FOM below 3 was achieved. Nonetheless, the excellent processability of these TCF-cyanines imparted through the use of polymer guest-host blends (25 wt%) allowed for the claddings of silicon-organic hybrid (SOH) waveguides (**Fig. 13a)** to be applied via a facile spin-casting method. On this basis, we successfully fabricated SOH waveguides based on **AJBC1723**, which can not only enable efficient optical wavelength conversion by four-wave mixing (FWM, **Fig. 13b**), but also optical power modulation via 2PA.

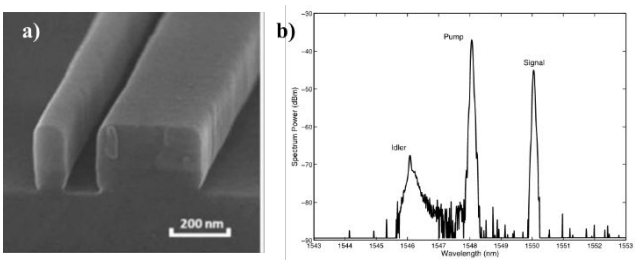

Fig. 13 a) SEM micrograph of the cross-section of a fabricated slotted waveguide with 100 nm and 310 nm width silicon rails, 180 nm slot width and 200 nm silicon rail thickness. b) Optical spectrum showing idler wavelength generated by near-degenerate four wave mixing in SOH waveguide coated with guest-host APC film doped with 25wt% of **AJBC1723**. Adopted from Ref. 109. Copyright, 2012, John Wiley and Sons.

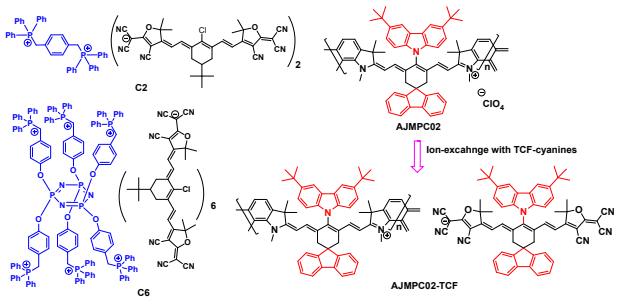

Fig 14. Chemical structures of cyanine complexes **C2** and **C6**, and conjugated polycyanine **AJMPC02** and its complementary cyanine slat complex **AJMPC02-TCF**.

To further understand the impact of counterions on the electronic structure of cyanines and their linear and NLO properties, we also used phosphonium-based counterions with multiple charges (di- and hexa-cations) to organize cyanines into multi-chromophore salt complexes (**C2** and **C6**, **Fig. 14**).[119] A study of the linear and NLO properties (**Table 4**) of these complexes over a large range of molecular concentrations was carefully conducted. We found the optical properties of hexa-cationic **C6** can endure much stronger intramolecular polymethine-counterion interactions, due to its spatially constrained geometry that could not provide as much freedom for the solvent molecules to effectively dissociate six cyanine units and hexa-cations, thereby inducing a higher local charge density. On the contrary, the optical properties of mono-cationic **AJBC1723** and di-cationic **C2** are more susceptible to chromophore-chromophore intermolecular interactions at high number density, while **C6** is encouragingly not immune to these interactions. Consequently, as shown in **Table 4**, **C6** can exhibit the highest $|\mathrm{Re}\chi^{(3)}|$ at both 1300 nm and 1550 nm, among these three complexes, although it has the smallest $|\mathrm{Re}(\gamma)|$. The above results strongly suggest the organization of cyanines into construct with multiple charges can provide a steric repulsive effect to mitigate the inter-complex interactions in the solid state, resulting in a more efficient translation between microscopic and macroscopic optical properties.

Table 4. Third-order NLO properties in solutions and neat films characterized by Z-scan method

No.	λ_{film}[a]	Excitation Wavelength [nm]	Re(γ) [10^{-32} esu]	$\lvert\mathrm{Re}(\gamma)/\mathrm{Im}(\gamma)\rvert$	Re$\chi^{(3)}$ [10^{-11} esu]	$\lvert\mathrm{Re}\chi^{(3)}/\mathrm{Im}\chi^{(3)}\rvert$
AJBC1723	936	1300	-1.3	7.8	-3.3	7.8
		1500	-1.6	1.6	-2.3	1.4
C2	936	1300	-1.2	7.1	-3.6	6.9
		1550	-1.2	1.6	-3.4	1.8
C6	936	1300	-0.88	5.1	-3.8	5.2
		1550	-1.0	1.7	-3.6	1.8
AJMPC02	960	1300	–7.3	1.2	/	/
AJMPC02-TCF	930	1300	-4.5	2.7	-15.0	1.5
		1550	/	/	6.1	0.7
PE1-TCF1	924	1300	-5.8	39	-1.6	≥20.0
		1550	-7.0	10.1	-2.8	≥9.2
PE1-TCF2	957	1300	-6.8	17.4	-15.5	≥7.4
Si<110>[b]	/	1270	/	/	0.81	3.5
		1540	/	/	1.3	4.6

[a] The maximum absorption wavelength as neat thin films. [b] From ref. 125.

As aforementioned, a Peierls-type symmetry breaking will occur for a cyanine if its L is greater than C9. A well-demonstrated solution is to use charge-stabilized end groups to enable more efficient delocalization of the π-electrons while still maintaining L < C9.[100, 120, 121] In 2015, we also reported an alternative approach to solve this problem by polymerizing cyanine molecules into fully conjugated polycyanines,[122] since it can provide extended exciton delocalization pathways beyond each individual cyanine unit along the polymeric chain. In our design, a simple indolium-based bi-functional "Janus core" and a substituted C7 conjugation bridge were used as the monomers to afford a new cationic polyindolinium (**AJMPC2**, **Fig. 14**) via a simple polycondensation. In order to improve the solubility/processability of polycyanine and also to mitigate adverse aggregation effects, two rigid and bulky substituents (carbazole and fluorene moieties) were introduced into the center of conjugation bridges as efficient spacers. As shown in **Fig. 15**, the absorption band of **AJMPC02** not only nicely retains the characteristics of highly polarizable and symmetric cyanines, but also shows a large bathochromic shift of 180 nm compared

This journal is © The Royal Society of Chemistry 20xx

Please do not adjust margins

to its monomeric cyanine, with an absorption centered at 1009 nm. The NLO properties of **AJMPC02** were studied by an accurate and sensitive Dual-Arm Z-scan technique[123], and as we expected, it shows an enhanced Re(γ) value of -7.3×10^{-32} $-7.3 \times 10^{-32} = -7.3 \times 10^{-32}$ esu at 1300 nm (**Table 4**) compared to those of indoline- and TCF-cyanines,[118, 124] indicating that γ can be enhanced significantly without a need of extending *L*. Moreover, considering **AJMPC02** can be seen as a conjugated polyelectrolyte and thus can be used as a host polymer to form complementary polymeric cyanine salt complexes with anionic cyanines, we further prepared **AJMPC02-TCF** (**Fig. 14**) by using TCF cyanines with the same conjugation bridge as the counterions for **AJMPC02**. In solution, this polymeric complex exhibits two absorption bands located at 900 nm and 1003 nm (**Fig. 15**), corresponding to the absorption of TCF cyanine and polycyanine, respectively. Encouragingly, it exhibits very good processability for device applications, and the resulting neat films possess a sharp absorption band with significantly reduced long-wavelength tail (**Fig. 15**), indicating the undesired ion-pairing and/or aggregation effects have been somewhat alleviated. As a result, neat films of **AJMPC02-TCF** can deliver one of the highest magnitudes of $|\mathrm{Re}\chi^{(3)}|$ among organic/inorganic NLO materials, 1.5×10^{-10} esu at 1300 nm and 6.1×10^{-11} esu at 1550 nm, respectively (**Table 4**). By comparison, as shown in **Table 4**, the magnitudes of $|\mathrm{Re}\chi^{(3)}|$ of bulk crystalline silicon along <110> direction were only determined to be 0.81×10^{-11} esu at 1270 nm and 1.3×10^{-11} esu at 1540 nm, respectively.[125]

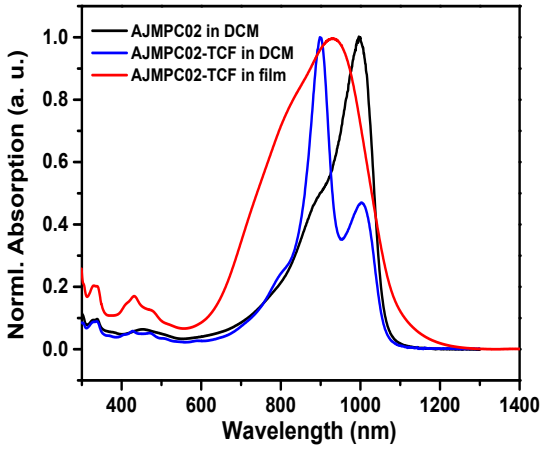

Fig. 15 Absorption spectra of **AJMPC02** and **AJMPC02-TCF** in dichloromethane (DCM) solutions, and as thin films for **AJMPC02-TCF**.

The above results clearly manifest that polyelectrolyte-cyanine salt complex could be an attractive material system to efficiently translate large γ to large $\mathrm{Re}\chi^{(3)}$ in films. However, we also note that the material FOM of AJMPC02-TCF is only ~1.5, much lower than that required by practical AOSP applications. Thus it is highly desirable for designing new polyelectrolyte-cyanine salt complexes that can reduce TPA loss while maintaining a large $|\mathrm{Re}\chi^{(3)}|$. To this end, we have rationally designed and synthesized a new phosphonium-based polyelectrolyte **PE1** by using the co-polyfluorene as a polymeric backbone via a "Click"-type polymer functionalization strategy, and through a simple ion-exchange with **PE1**, two polyelectrolyte-cyanine complexes **PE1-TCF1** and **PE1-TCF2** were then obtained as shown in **Fig. 16a**.[116] Bis-4-fluorophenyl functionalized TCF end-groups in the cyanines of **PE1-TCF2** can enhance the electron-withdrawing strength of end groups, leading to a red shift of ~35 nm in the absorption maximum (**Fig. 16b**). It is encouragingly found that the use of cationic **PE1** as the host polymer for TCF-cyanines can significantly reduce the strong and random aggregations between cyanines in the solid state by comparing their absorption spectra with that of guest-host films of **AJBC1723** with similar effective chromophore density (**Fig. 16c**), which could be attributed to an efficient dispersion of TCF-cyanines into polyelectrolyte via Coulombic interactions. Such favorable dispersion effect thus can help to effectively translate large γ of cyanines to large $\mathrm{Re}\chi^{(3)}$ in high number density films as shown in **Table 4**. The material FOMs of **PE1-TCF1** were found to be larger than 20 at 1300 nm and larger than 9.2 at 1550 nm, both of which even are comparable to the corresponding |Re(γ)/Im(γ)| ratios. More encouragingly, at 1550 nm, **PE1-TCF2** exhibits one of the largest $|\mathrm{Re}\chi^{(3)}|$ values of 1.55 × 10^{-10} esu with a material FOM of greater than 7.4, among the best for organic/inorganic third-order NLO materials in this spectral window. In addition to favorable dispersion effect derived from the host polyelectrolyte, the higher NLO effects for **PE1-TCF2** could be also due to its bis-4-fluorophenyl substituents in the TCF end-groups, which can act as effective spacers to prevent the cyanine aggregations.

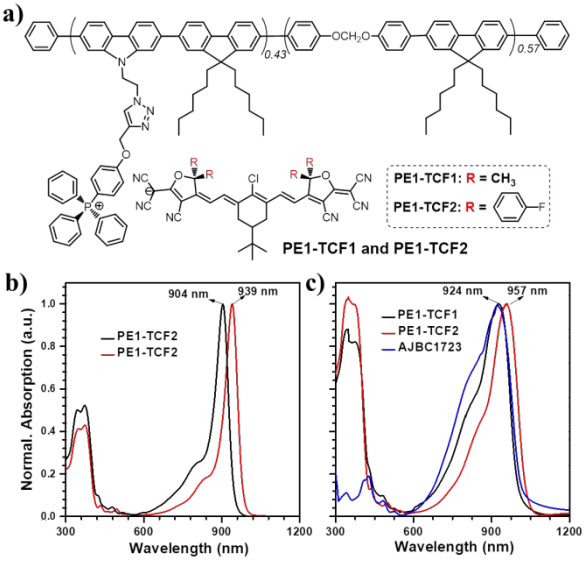

Fig. 16 a) Chemical structures of polyelectrolyte-cyanine complexes (**PE1-TCF1** and **PE1-TCF2**); Absorption spectra of **PE1-TCF1** and **PE1-TCF2** in diluted DCM solutions (b) and neat thin films (c), while guest-host film absorption of **AJBC1723** in APC (50wt%) was provided for comparison.

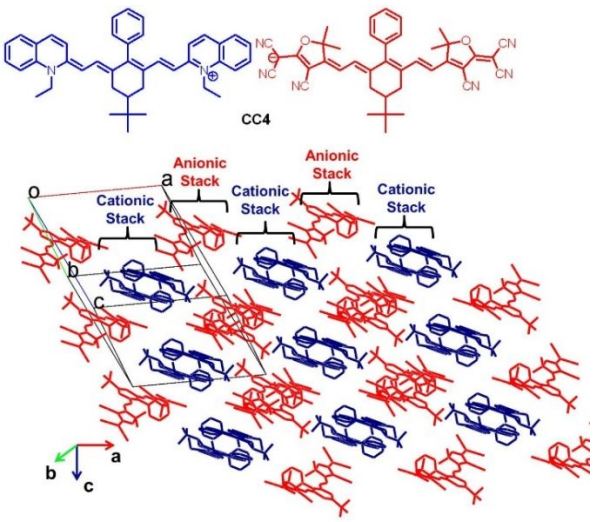

Fig 17. Chemical structure of complementary cyanine-cyanine salt **CC4** and its crystal structure viewed along *b*-axis. Adopted from Ref. 120. Copyright, 2015, American Chemical Society.

As discussed above, random aggregations have been shown to play a significantly negative role, however, we believe well-controlled J-aggregates should be useful for achieving large $\chi^{(3)}$, given the fact that the exciton delocalization can occur among molecules in J-aggregates to enable sizable enhancement of the nonlinearities.[126, 127] Furthermore, as well-known the absorption band induced by J-aggregates is particularly very sharp,[128] potentially reducing the linear optical loss if controlling them in the suitable optical window. However, self-assembly of cyanines with long conjugation length ($L \geq 7$) into the J-aggregate form remains a big challenge, although the discovery of the dye J-aggregate was from a cyanine, i. e. pseudoisocyanine (PIC).[129] Moreover, it is also very challenging to achieve J-aggregates in the solid state rather than in solution. Due to the ionic nature of cyanines, we recently proposed a new design strategy that can achieve supramolecular J-aggregates of highly polarizable TCF-heptamethines in the crystal state by organizing anionic and cationic cyanines into complementary salts.[130] We designed a cationic quinolinium-heptamethine with phenyl substituent at the center of conjugation bridge as the counterion as the anionic TCF-heptamethine with the same conjugation bridge, and in the crystal structure of resulting complementary salt **CC4**, the oppositely-charged cyanines clearly form a cooperative self-assembly and individually pack in alternating J-type fashion (**Fig. 17**). In addition, both cationic and anionic cyanines in the **CC4** can maintain overall symmetric geometries in the crystal state, and thus their BLAs were calculated to be only 0.015 Å and 0.020 Å, respectively, much smaller than those reported in literatures. Nonetheless, we have to note that we could not grow sufficiently large size crystals containing J-aggregates and also we could not find any effective approaches that can keep these favorable J-aggregates in the optical quality films, thereby limiting their further AOSP applications. Nonetheless, our work has provided a good understanding of the structural properties of the cyanine aggregates at the molecular level.

Conclusions

In summary, this review highlights the recent advances of organic second-order and third-order NLO materials. With regard to the current research status and application prospects of EO polymers, our research emphasizes on how to improve the synthesis efficiency of chromophores to achieve the large-scale and cost-effective synthesis. Multi-component condensation methods can significantly shorten synthetic time and have high yields. Combining multicomponent condensation methods with supramolecular self-assembly techniques holds the promise of future rapid and concise mass synthesis of high-performance self-assembled chromophores. Processing and efficient poling of EO polymer films are key to advancing their applications. we have investigated the regulation of the dielectric constant by nano-doping, preparation and large-area poling of EO polymer on soda-lime glasses and the development of low optical loss graphene electrode to replace metal electrodes for electric field poling. These efforts are expected to facilitate the efficient poling of EO polymers in different type of waveguide devices. Over the past two decades we have witnessed continuous breakthroughs in the performance of electro-optic polymer materials. Device applications of the EO materials are also being pursued in recent years, which requires the efforts and cooperation of material and device researchers. We predict that the future development of electro-optic polymers will focus on the following two points:

1) It is highly urgent to further improve the processability of the materials and develop electro-optic polymers with high chemical stability against acid/alkali and high thermal stability at 85 °C. This is a challenge that must be addressed for a wide range of applications in EO waveguide devices;

2) The performance of organic EO materials and hybrid devices have increased remarkably in recent years, making them an exciting prospect for the launch of 5G/6G technology. However, the progressive research and development of organic EO materials have been harmed by the lack of reliable EO characterization techniques and in-depth understanding of structure-property relationship. Similar to a few other research fields of optoelectronic materials and devices, frequent occurrence of incorrect and unreliable data-reporting of ultrahigh EO coefficients risks damaging the credibility and reliability of the field. For any new thin film EO materials, it is essential to present a complete set of data based on the experimental data and the details of data analysis, including the EO measurement, the poling-induced birefringences or absorption change, order parameters, dielectric properties and thermal stability, *etc*. Independent evaluation based on the results of thin films, slab waveguides and EO devices should be continuously updated to complete the database of high performance organic EO materials and eliminate the ones with poor reproducibility and reliability. Furthermore, it is necessary to analyse the intrinsic hyperpolarizabilities of chromophores from the experimental measurements in solutions and poled films with the help of computational analysis, so that for a given D-pi-A structure, the upper limit of materials' EO performance

This journal is © The Royal Society of Chemistry 20xx

Please do not adjust margins

can be quantitatively justified based on the number density and poling efficiency of the materials.

For cyanine-based organic AOSP materials, although an encouraging research progress has been made now by rationally designing the structure of counterions and/or introducing bulky, rigid spacers into cyanines to reduce undesired ion-pairing and aggregation effects, it seems that achievement of a large $|\mathrm{Re}\chi^{(3)}|$ magnitude beyond 10^{-10} esu with a high material FOM over 12 still remains a significant challenge in the field. Based on our previous work,[107] the construction of polyelectrolyte-cyanine complexes could be a promising approach. However, we think the use of polyelectrolyte to achieve homogenous dispersion of cyanines does not fully realize its value. As mentioned above, not all aggregates necessarily paly a negative role in the solid-state third-order NLO properties, and highly-ordered J-aggregates with suitable absorption window should be very useful. Since one attractive feature of polyelectrolytes is their templating effect in achieving a supramolecular assembly, we hope future efforts will be devoted to designing new polyelectrolytes that can assemble these cyanines with large γ into J-aggregates in optical quality composite films. Moreover, we also expect other material systems having high third-order NLO performance like cyanines can be developed.

Aside from the material design, the future of organic NLO materials should also focus on broadening their applications in diverse organic-inorganic hybrid waveguide systems. The rational design, high throughput processing and device engineering of highly performance organic NLO materials, will leverage mature manufacturing infrastructure of electronics, to be fed into the development of major integrated photonic platforms, including silicon photonics, plasmonics, and dielectric waveguides of sol-gel silica and polymers. It will also benefit a broad spectrum of technologies in telecommunications, computation systems, spectroscopy, and remote sensing/imaging systems. In particular, the development can meet the huge demand for expansion and speed-up of optical interconnect technology, providing new high-bandwidth, low-energy information processing systems for the next generation of 5G mobile wireless communication systems, data centers, laser radar, Terahertz communication and sensing, as well as enterprise networks.

Conflicts of interest

There are no conflicts to declare.

Acknowledgements

This review is dedicated to Professor Tobin J. Marks on the occasion of his 75th birthday, in recognition of his outstanding contribution to organic second-order and third-order nonlinear optical materials. The research in second-order NLO materials was supported by grants from Natural Science Foundation of China (21975213), Shenzhen Science & Technology Innovation Committee (JCYJ20180507181718203), General Research Fund of HKSAR (RGC Ref No. 11306320), Fundamental Research Funds for the Central Universities (ZYGX2019Z005), APRC-CityU New Research Initiatives/Infrastructure Support from Central (Project 9610389), Air Force Office of Scientific Research (FA8650-14-C-5005). We are grateful to the following collaborators for their outstanding work in second-order NLO materials and devices: Professors Robert Norwood and Nasser Peyghambarian (University of Arizona), Ray T. Chen (University of Texas at Austin and Omega Optics), Larry Dalton and Bruce Robinson (University of Washington), L. Michael Hayden (University of Maryland, Baltimore County), Enami Yasufumi (Nagasaki University), Alan Wang (Oregon State University), Amir H. Safavi-Naeini (Stanford University), Manfred Eich (Hamburg University of Technology), Christian Koos and Wolfgang Freude (Karlsruhe Institute of Technology), Ming Li (Changchun University of Technology), Zhanchen Cui (Jilin University), Kin Seng Chiang (City University of Hong Kong), Kaixin Chen (University of Electronic Science and Technology of China), Harish Subbaraman (Boise State University), Dr. Dong-Hun Park (Laboratory for Physical Sciences). This work related to third-order NLO materials was supported by grants from the AFOSR MURI (FA9550–10–1–0558); the DARPA ZOE Program (W31P4Q-09-1-0012). We also appreciate our collaborators Joseph W. Perry, Seth R. Marder and Jean-Luc Brédas (Georgia Institute of Technology), David J. Hagan and Eric W. Van Stryland (University of Central Florida), Robert Norwood and Nasser Peyghambarian (University of Arizona).

Notes and references

1. J. Hecht, *Nature*, 2016, **536**, 139-142.
2. J. Witzens, *Nature Photonics*, 2017, **11**, 459-462.
3. M. Hilbert and P. Lopez, *Science*, 2011, **332**, 60-65.
4. W. Heni, Y. Kutuvantavida, C. Haffner, H. Zwickel, C. Kieninger, S. Wolf, M. Lauermann, Y. Fedoryshyn, A. F. Tillack, L. E. Johnson, D. L. Elder, B. H. Robinson, W. Freude, C. Koos, J. Leuthold and L. R. Dalton, *Acs Photonics*, 2017, **4**, 1576-1590.
5. C. Koos, J. Leuthold, W. Freude, M. Kohl, L. Dalton, W. Bogaerts, A. L. Giesecke, M. Lauermann, A. Melikyan, S. Koeber, S. Wolf, C. Weimann, S. Muehlbrandt, K. Koehnle, J. Pfeifle, W. Hartmann, Y. Kutuvantavida, S. Ummethala, R. Palmer, D. Korn, L. Alloatti, P. C. Schindler, D. L. Elder, T. Wahlbrink and J. Bolten, *Journal of Lightwave Technology*, 2016, **34**, 256-268.
6. J. L. Liu, G. M. Xu, F. G. Liu, I. Kityk, X. H. Liua and Z. Zhen, *Rsc Advances*, 2015, **5**, 15784-15794.
7. Y. Q. Shi, C. Zhang, H. Zhang, J. H. Bechtel, L. R. Dalton, B. H. Robinson and W. H. Steier, *Science*, 2000, **288**, 119-122.
8. M. Lee, H. E. Katz, C. Erben, D. M. Gill, P. Gopalan, J. D. Heber and D. J. McGee, *Science*, 2002, **298**, 1401-1403.
9. C. L. Hu, Z. Chen, H. Y. Xiao, Z. Zhen, X. H. Liu and S. H. Bo, *J Mater Chem C*, 2017, **5**, 5111-5118.
10. Y. H. Yang, H. J. Xu, F. G. Liu, H. R. Wang, G. W. Deng, P. Si, H. Y. Huang, S. H. Bo, J. L. Liu, L. Qiu, Z. Zhen and X. H. Liu, *J Mater Chem C*, 2014, **2**, 5124-5132.
11. H. Zhang, Y. H. Yang, H. Y. Xiao, F. G. Liu, F. Y. Huo, L. Chen, Z. Chen, S. H. Bo, L. Qiu and Z. Zhen, *J Mater Chem C*, 2017, **5**, 6704-6712.
12. Y. L. He, L. Chen, H. Zhang, Z. Chen, F. Y. Huo, B. Li, Z. Zhen, X. H. Liu and S. H. Bo, *J Mater Chem C*, 2018, **6**, 1031-1037.
13. R. L. Tang and Z. Li, *Chemical Record*, 2017, **17**, 71-89.
14. J. D. Luo, X. H. Zhou and A. K. Y. Jen, *J Mater Chem*, 2009, **19**, 7410-7424.

15. M. Li, Y. Li, H. Zhang, S. W. Wang, Y. H. Ao and Z. C. Cui, *Journal of Materials Chemistry C*, 2017, **5**, 4111-4122.
16. R. Tang, S. Zhou, Z. Cheng, G. Yu, Q. Peng, H. Zeng, G. Guo, Q. Li and Z. Li, *Chem. Sci.*, 2017, **8**, 340-347.
17. Z. Li, W. Wu, G. Yu, Y. Liu, C. Ye, J. Qin and Z. Li, *ACS Appl. Mater. Interfaces*, 2009, **1**, 856-863.
18. Z. Li, W. Wu, Q. Li, G. Yu, L. Xiao, Y. Liu, C. Ye, J. Qin and Z. Li, *Angew. Chem. Int. Ed.*, 2010, **49**, 2763-2767.
19. X. Zang, G. Liu, Q. Li, Z. a. Li and Z. Li, *Macromolecules*, 2020, **53**, 4012-4021.
20. D. Marpaung, J. P. Yao and J. Capmany, *Nat Photonics*, 2019, **13**, 80-90.
21. C. Haffner, D. Chelladurai, Y. Fedoryshyn, A. Josten, B. Baeuerle, W. Heni, T. Watanabe, T. Cui, B. J. Cheng, S. Saha, D. L. Elder, L. R. Dalton, A. Boltasseva, V. M. Shalaev, N. Kinsey and J. Leuthold, *Nature*, 2018, **556**, 483-+.
22. A. Woessner, Y. D. Gao, I. Torre, M. B. Lundeberg, C. Tan, K. Watanabe, T. Taniguchi, R. Hillenbrand, J. Hone, M. Polini and F. H. L. Koppens, *Nat Photonics*, 2017, **11**, 421-424.
23. Y. Ding, X. Guan, X. Zhu, H. Hu, S. I. Bozhevolnyi, L. K. Oxenlowe, K. J. Jin, N. A. Mortensen and S. Xiao, *Nanoscale*, 2017, **9**, 15576-15581.
24. A. Melikyan, L. Alloatti, A. Muslija, D. Hillerkuss, P. C. Schindler, J. Li, R. Palmer, D. Korn, S. Muehlbrandt, D. Van Thourhout, B. Chen, R. Dinu, M. Sommer, C. Koos, M. Kohl, W. Freude and J. Leuthold, *Nat Photonics*, 2014, **8**, 229-233.
25. M. Ayata, Y. Fedoryshyn, W. Heni, B. Baeuerle, A. Josten, M. Zahner, U. Koch, Y. Salamin, C. Hoessbacher, C. Haffner, D. L. Elder, L. R. Dalton and J. Leuthold, *Science*, 2017, **358**, 630-632.
26. W. Heni, Y. Fedoryshyn, B. Baeuerle, A. Josten, C. B. Hoessbacher, A. Messner, C. Haffner, T. Watanabe, Y. Salamin, U. Koch, D. L. Elder, L. R. Dalton and J. Leuthold, *Nat Commun*, 2019, **10**.
27. S. Ummethala, T. Harter, K. Koehnle, Z. Li, S. Muehlbrandt, Y. Kutuvantavida, J. Kemal, P. Marin-Palomo, J. Schaefer, A. Tessmann, S. K. Garlapati, A. Bacher, L. Hahn, M. Walther, T. Zwick, S. Randel, W. Freude and C. Koos, *Nat Photonics*, 2019, **13**, 519-522.
28. J. H. Wulbern, S. Prorok, J. Hampe, A. Petrov, M. Eich, J. D. Luo, A. K. Y. Jen, M. Jenett and A. Jacob, *Optics Letters*, 2010, **35**, 2753-2755.
29. X. L. Wang, C. Y. Lin, S. Chakravarty, J. D. Luo, A. K. Y. Jen and R. T. Chen, *Opt Lett*, 2011, **36**, 882-884.
30. L. Alloatti, R. Palmer, S. Diebold, K. P. Pahl, B. Q. Chen, R. Dinu, M. Fournier, J. M. Fedeli, T. Zwick, W. Freude, C. Koos and J. Leuthold, *Light-Science & Applications*, 2014, **3**, e173.
31. M. Lauermann, S. Wolf, P. C. Schindler, R. Palmer, S. Koeber, D. Korn, L. Alloatti, T. Wahlbrink, J. Bolten, M. Waldow, M. Koenigsmann, M. Kohler, D. Malsam, D. L. Elder, P. V. Johnston, N. Phillips-Sylvain, P. A. Sullivan, L. R. Dalton, J. Leuthold, W. Freude and C. Koos, *Journal of Lightwave Technology*, 2015, **33**, 1210-1216.
32. M. Lauermann, S. Wolf, W. Hartmann, R. Palmer, Y. Kutuvantavida, H. Zwickel, A. Bielik, L. Altenhain, J. Lutz, R. Schmid, T. Wahlbrink, J. Bolten, A. L. Giesecke, W. Freude and C. Koos, *Optics Express*, 2016, **24**, 9389-9396.
33. H. Yan, X. C. Xu, C. J. Chung, H. Subbaraman, Z. Y. Pan, S. Chakravarty and R. T. Chen, *Opt Lett*, 2016, **41**, 5466-5469.
34. C. Kieninger, Y. Kutuvantavida, D. L. Elder, S. Wolf, H. Zwickel, M. Blaicher, J. N. Kemal, M. Lauermann, S. Randel, W. Freude, L. R. Dalton and C. Koos, *Optica*, 2018, **5**, 739-748.
35. F. Qiu, A. M. Spring, F. Yu, I. Aoki, A. Otomo and S. Yokoyama, *Laser Photonics Rev*, 2013, **7**, L84-L88.
36. F. Qiu, A. M. Spring, H. Miura, D. Maeda, M. A. Ozawa, K. Odoi and S. Yokoyama, *Acs Photonics*, 2016, **3**, 780-783.
37. F. Qiu, A. M. Spring, J. X. Hong, H. Miura, T. Kashino, T. Kikuchi, M. Ozawa, H. Nawata, K. Odoi and S. Yokoyama, *Laser Photonics Rev*, 2017, **11**, 1700061.
38. H. Miura, F. Qiu, A. M. Spring, T. Kashino, T. Kikuchi, M. Ozawa, H. Nawata, K. Odoi and S. Yokoyama, *Opt Express*, 2017, **25**, 28643-28649.
39. X. Y. Zhang, A. Hosseini, S. Chakravarty, J. D. Luo, A. K. Y. Jen and R. T. Chen, *Opt Lett*, 2013, **38**, 4931-4934.
40. X. Y. Zhang, C. J. Chung, A. Hosseini, H. Subbaraman, J. D. Luo, A. K. Y. Jen, R. L. Nelson, C. Y. C. Lee and R. T. Chen, *J Lightwave Technol*, 2016, **34**, 2941-2951.
41. R. Himmelhuber, R. A. Norwood, Y. Enami and N. Peyghambarian, *Sensors-Basel*, 2015, **15**, 18239-18255.
42. Y. Enami, H. Nakamura, J. Luo and A. K. Y. Jen, *Opt Commun*, 2016, **362**, 77-80.
43. Y. Enami, D. Mathine, C. T. DeRose, R. A. Norwood, J. Luo, A. K. Y. Jen and N. Peyghambarian, *Appl Phys Lett*, 2009, **94**, 213513.
44. Y. Enami, D. Mathine, C. T. DeRose, R. A. Norwood, J. Luo, A. K. Y. Jen and N. Peyghambarian, *Appl Phys Lett*, 2008, **92**, 193508.
45. Y. Enami, Y. Kayaba, J. D. Luo and A. K. Y. Jen, *Opt Express*, 2014, **22**, 16418-16423.
46. Y. Enami, Y. Jouane, J. D. Luo and A. K. Y. Jen, *Opt Express*, 2014, **22**, 30191-30199.
47. Y. Enami, C. T. Derose, D. Mathine, C. Loychik, C. Greenlee, R. A. Norwood, T. D. Kim, J. Luo, Y. Tian, A. K. Y. Jen and N. Peyghambarian, *Nat Photonics*, 2007, **1**, 423-423.
48. S. B. Shiring, R. L. Gieseking, C. Risko and J. L. Bredas, *J Phys Chem C*, 2017, **121**, 14166-14175.
49. J. M. Hales, S. Barlow, H. Kim, S. Mukhopadhyay, J. L. Bredas, J. W. Perry and S. R. Marder, *Chem Mater*, 2014, **26**, 549-560.
50. S. R. Marder, *MRS Bulletin*, 2016, **41**, 53-62.
51. M. Hochberg, T. Baehr-Jones, G. X. Wang, M. Shearn, K. Harvard, J. D. Luo, B. Q. Chen, Z. W. Shi, R. Lawson, P. Sullivan, A. K. Y. Jen, L. Dalton and A. Scherer, *Nature Materials*, 2006, **5**, 703-709.
52. C. Koos, P. Vorreau, T. Vallaitis, P. Dumon, W. Bogaerts, R. Baets, B. Esembeson, I. Biaggio, T. Michinobu, F. Diederich, W. Freude and J. Leuthold, *Nat Photonics*, 2009, **3**, 216-219.
53. S. R. Marder, J.-L. Brédas and J. W. Perry, *MRS Bulletin*, 2007, **32**, 561-565.
54. R. L. Gieseking, S. Mukhopadhyay, C. Risko, S. R. Marder and J. L. Bredas, *Adv. Mater.*, 2014, **26**, 68-83.
55. J. Leuthold, C. Koos and W. Freude, *Nat. Photonics*, 2010, **4**, 535-544.
56. J. M. Hales, S. Barlow, H. Kim, S. Mukhopadhyay, J.-L. Brédas, J. W. Perry and S. R. Marder, *Chem. Mater.*, 2014, **26**, 549-560.
57. Q. Q. Li and Z. Li, *Accounts Chem Res*, 2020, **53**, 962-973.
58. W. B. Wu, R. L. Tang, Q. Q. Li and Z. Li, *Chem Soc Rev*, 2015, **44**, 3997-4022.
59. A. J. T. Lou, S. Righetto, C. Barger, C. Zuccaccia, E. Cariati, A. Macchioni and T. J. Marks, *J Am Chem Soc*, 2018, **140**, 8746-8755.
60. S. Liu, M. A. Haller, H. Ma, L. R. Dalton, S. H. Jang and A. K. Y. Jen, *Adv Mater*, 2003, **15**, 603-607.
61. L. R. Dalton, P. A. Sullivan and D. H. Bale, *Chem. Rev.*, 2010, **110**, 25-55.
62. H. Kang, A. Facchetti, H. Jiang, E. Cariati, S. Righetto, R. Ugo, C. Zuccaccia, A. Macchioni, C. L. Stern, Z. F. Liu, S. T. Ho, E. C. Brown, M. A. Ratner and T. J. Marks, *J Am Chem Soc*, 2007, **129**, 3267-3286.
63. G. Bourhill, J. L. Bredas, L. T. Cheng, S. R. Marder, F. Meyers, J. W. Perry and B. G. Tiemann, *J Am Chem Soc*, 1994, **116**, 2619-2620.
64. Y. J. Cheng, J. D. Luo, S. Hau, D. H. Bale, T. D. Kim, Z. W. Shi, D. B. Lao, N. M. Tucker, Y. Q. Tian, L. R. Dalton, P. J. Reid and A. K. Y. Jen, *Chemistry of Materials*, 2007, **19**, 1154-1163.
65. J. D. Luo, Y. J. Cheng, T. D. Kim, S. Hau, S. H. Jang, Z. W. Shi, X. H. Zhou and A. K. Y. Jen, *Organic Letters*, 2006, **8**, 1387-1390.
66. J. D. Luo, S. Huang, Y. J. Cheng, T. D. Kim, Z. W. Shi, X. H. Zhou and A. K. Y. Jen, *Organic Letters*, 2007, **9**, 4471-4474.
67. C. Zhang, L. R. Dalton, M. C. Oh, H. Zhang and W. H. Steier, *Chem Mater*, 2001, **13**, 3043-3050.

This journal is © The Royal Society of Chemistry 20xx

Please do not adjust margins

68. J. Luo, F. Lin, Z. A. Li, M. Li, T. D. Kim, S. H. Jang and A. K. Y. Jen, *J Mater Chem C*, 2017, **5**, 2230-2234.
69. W. Bentoumi, J. C. Mulatier, P. A. Bouit, O. Maury, A. Barsella, J. P. Vola, E. Chastaing, L. Divay, F. Soyer, P. Le Barny, Y. Bretonniere and C. Andraud, *Chem-Eur J*, 2014, **20**, 8909-8913.
70. H. J. Xu, J. P. Liu, J. Liu, C. W. Yu, Z. F. Zhai, G. Z. Qina and F. G. Liu, *Mater Chem Front*, 2020, **4**, 168-175.
71. T. D. Kim, J. W. Kang, J. D. Luo, S. H. Jang, J. W. Ka, N. Tucker, J. B. Benedict, L. R. Dalton, T. Gray, R. M. Overney, D. H. Park, W. N. Herman and A. K. Y. Jen, *J Am Chem Soc*, 2007, **129**, 488-489.
72. X. H. Zhou, J. D. Luo, S. Huang, T. D. Kim, Z. W. Shi, Y. J. Cheng, S. H. Jang, D. B. Knorr, R. M. Overney and A. K. Y. Jen, *Adv Mater*, 2009, **21**, 1976-1981.
73. J. Y. Wu, B. Wu, W. Wang, K. S. Chiang, A. K. Y. Jen and J. D. Luo, *Conf Laser Electr*, 2018.
74. J. Y. Wu, B. Wu, W. Wang, K. S. Chiang, A. K. Y. Jen and J. D. Luo, *Mater Chem Front*, 2018, **2**, 1046-1046.
75. M. Li, S. Huang, X. H. Zhou, Y. Zang, J. Y. Wu, Z. C. Cui, J. D. Luo and A. K. Y. Jen, *J Mater Chem C*, 2015, **3**, 6737-6744.
76. D. L. Elder, C. Haffner, W. Heni, Y. Fedoryshyn, K. E. Garrett, L. E. Johnson, R. A. Campbell, J. D. Avila, B. H. Robinson, J. Leuthold and L. R. Dalton, *Chem Mater*, 2017, **29**, 6457-6471.
77. H. J. Xu, D. L. Elder, L. E. Johnson, B. H. Robinson and L. R. Dalton, *Acs Appl Mater Inter*, 2019, **11**, 21058-21068.
78. Y. Enami, G. Meredith, N. Peyghambarian, M. Kawazu and A. K. Y. Jen, *Appl Phys Lett*, 2003, **82**, 490-492.
79. R. A. Norwood, C. Derose, Y. Enami, H. Gan, C. Greenlee, R. Himmelhuber, O. Kropachev, C. Loychik, D. Mathine, Y. Merzylak, M. Fallahi and N. Peyghambarian, *J Nonlinear Opt Phys*, 2007, **16**, 217-230.
80. S. Huang, J. D. Luo, H. L. Yip, A. Ayazi, X. H. Zhou, M. Gould, A. Chen, T. Baehr-Jones, M. Hochberg and A. K. Y. Jen, *Adv Mater*, 2012, **24**, Op42-Op47.
81. S. Huang, J. D. Luo, Z. A. Jin, M. Li, T. D. Kim, A. T. Chen and A. K. Y. Jen, *Appl Phys Lett*, 2014, **105**, 183305.
82. W. W. Jin, P. V. Johnston, D. L. Elder, K. T. Manner, K. E. Garrett, W. Kaminsky, R. M. Xu, B. H. Robinson and L. R. Dalton, *J Mater Chem C*, 2016, **4**, 3119-3124.
83. W. W. Jin, P. V. Johnston, D. L. Elder, A. F. Tillack, B. C. Olbricht, J. S. Song, P. J. Reid, R. M. Xu, B. H. Robinson and L. R. Dalton, *Appl Phys Lett*, 2014, **104**, 243304.
84. H. J. Xu, F. G. Liu, D. L. Elder, L. E. Johnson, Y. de Coene, K. Clays, B. H. Robinson and L. R. Dalton, *Chem Mater*, 2020, **32**, 1408-1421.
85. Y. F. Li, *Accounts Chem Res*, 2012, **45**, 723-733.
86. J. Y. Wu, J. D. Luo, N. Cernetic, K. X. Chen, K. S. Chiang and A. K. Y. Jen, *J Mater Chem C*, 2016, **4**, 10286-10292.
87. J. D. Luo, D. H. Park, R. Himmelhuber, Z. L. Zhu, M. Li, R. A. Norwood and A. K. Y. Jen, *Opt Mater Express*, 2017, **7**, 1909-1916.
88. W. Wang, J. Y. Wu, K. X. Chen, Q. D. Huang, J. D. Luo and K. S. Chiang, *Opt Lett*, 2020, **45**, 2383-2386.
89. D. H. Park, V. Yun, J. Luo, A. K. Y. Jen and W. N. Herman, *Electron Lett*, 2016, **52**, 1703-1705.
90. J. D. Witmer, T. P. McKenna, P. Arrangoiz-Arriola, R. Van Laer, E. A. Wollack, F. C. Lin, A. K. Y. Jen, J. D. Luo and A. H. Safavi-Naeini, *Quantum Sci Technol*, 2020, **5**, 034004.
91. S. Wolf, H. Zwickel, W. Hartmann, M. Lauermann, Y. Kutuvantavida, C. Kieninger, L. Altenhain, R. Schmid, J. D. Luo, A. K. Y. Jen, S. Randel, W. Freude and C. Koos, *Scientific Reports*, 2018, **8**.
92. H. Zwickel, S. Wolf, C. Kieninger, Y. Kutuvantavida, M. Lauermann, T. de Keulenaer, A. Vyncke, R. Vaernewyck, J. D. Luo, A. K. Y. Jen, W. Freude, J. Bauwelinck, S. Randel and C. Koos, *Opt Express*, 2017, **25**, 23784-23800.
93. Z. Y. Pan, X. C. Xu, C. J. Chung, H. Dalir, H. Yan, K. Chen, Y. G. Wang, B. H. Jia and R. T. Chen, *Laser Photonics Rev*, 2018, **12**, 1700300.
94. Z. Y. Pan, X. C. Xu, C. J. Chung, H. Dalir, H. Yan, K. Chen, Y. G. Wang and R. T. Chen, *2018 Optical Fiber Communications Conference and Exposition (Ofc)*, 2018.
95. H. Yan, X. C. Xu, C. J. Chung, H. Subbaraman, Z. Y. Pan, S. Chakravarty and R. T. Chen, *Proc Spie*, 2017, **10109**.
96. Y. Enami, A. Seki, S. Masuda, T. Joichi, J. D. Luo and A. K. Y. Jen, *J Lightwave Technol*, 2018, **36**, 4181-4189.
97. D. Park, V. R. Pagan, P. S. Cho, J. D. Luo, A. K. Y. Jen and P. V. Petruzzi, *Opt Express*, 2017, **25**, 29885-29895.
98. F. H. Ren, M. Li, Q. Gao, W. Cowell, J. D. Luo, A. K. Y. Jen and A. X. Wang, *Opt Commun*, 2015, **352**, 116-120.
99. G. I. Stegeman and R. H. Stolen, *J. Opt. Soc. Am. B*, 1989, **6**, 652-662.
100. J. M. Hales, J. Matichak, S. Barlow, S. Ohira, K. Yesudas, J. L. Bredas, J. W. Perry and S. R. Marder, *Science*, 2010, **327**, 1485-1488.
101. A. Mishra, R. K. Behera, P. K. Behera, B. K. Mishra and G. B. Behera, *Chem. Rev.*, 2000, **100**, 1973-2012.
102. F. Meyers, S. R. Marder, B. M. Pierce and J. L. Bredas, *J. Am. Chem. Soc.*, 1994, **116**, 10703-10714.
103. T. Johr, W. Werncke, M. Pfeiffer, A. Lau and L. Dähne, *Chem. Phys. Lett.*, 1995, **246**, 521-526.
104. L. M. Tolbert and X. Zhao, *J. Am. Chem. Soc.*, 1997, **119**, 3253-3258.
105. H. Hu, O. V. Przhonska, F. Terenziani, A. Painelli, D. Fishman, T. R. Ensley, M. Reichert, S. Webster, J. L. Bricks and A. D. Kachkovski, *Phys. Chem. Chem. Phys.*, 2013, **15**, 7666-7678.
106. A. E. Masunov, D. Anderson, A. Y. Freidzon and A. A. Bagaturyants, *J. Phys. Chem. A*, 2015, **119**, 6807-6815.
107. A. Scarpaci, A. Nantalaksaku, J. M. Hales, J. D. Matichak, S. Barlow, M. Rumi, J. W. Perry and S. R. Marder, *Chem. Mater.*, 2012, **24**, 1606-1618.
108. S. Mukhopadhyay, C. Risko, S. R. Marder and J.-L. Bredas, *Chem. Sci.*, 2012, **3**, 3103-3112.
109. R. L. Gieseking, S. Mukhopadhyay, S. B. Shiring, C. Risko and J.-L. Brédas, *J. Phys. Chem. C*, 2014, **118**, 23575-23585.
110. R. L. Gieseking, S. Mukhopadhyay, C. Risko, S. R. Marder and J.-L. Brédas, *Chem. Mater.*, 2014, **26**, 6439-6447.
111. P. A. Bouit, C. Aronica, L. Toupet, B. Le Guennic, C. Andraud and O. Maury, *J. Am. Chem. Soc.*, 2010, **132**, 4328-4335.
112. S. Barlow, J.-L. Bredas, Y. A. Getmanenko, R. L. Gieseking, J. M. Hales, H. Kim, S. R. Marder, J. W. Perry, C. Risko and Y. Zhang, *Mater. Horiz.*, 2014, **1**, 577-581.
113. Y. A. Getmanenko, T. G. Allen, H. Kim, J. M. Hales, B. Sandhu, M. S. Fonari, K. Y. Suponitsky, Y. Zhang, V. N. Khrustalev, J. D. Matichak, T. V. Timofeeva, S. Barlow, S.-H. Chi, J. W. Perry and S. R. Marder, *Adv. Funct. Mater.*, 2018, **28**, 1804073.
114. I. Davydenko, S. Barlow, R. Sharma, S. Benis, J. Simon, T. G. Allen, M. W. Cooper, V. Khrustalev, E. V. Jucov and R. l. Castañeda, *J. Am. Chem. Soc.*, 2016, **138**, 10112-10115.
115. I. Davydenko, S. Benis, S. B. Shiring, J. Simon, R. Sharma, T. G. Allen, S.-H. Chi, Q. Zhang, Y. A. Getmanenko, T. C. Parker, J. W. Perry, J.-L. Brédas, D. J. Hagan, E. W. Van Stryland, S. Barlow and S. R. Marder, *J. Mater. Chem. C*, 2018, **6**, 3613-3620.
116. Z. a. Li, A. A. Syed, P. Zhao, J. C. Yang, R. Sharma, T. R. Ensley, J. D. Matichak, I. Davydenko, S.-H. Jang and D. J. Hagan, *J. Am. Chem. Soc.*, 2019, **141**, 17331-17336.
117. P. A. Bouit, E. Di Piazza, S. Rigaut, B. Le Guennic, C. Aronica, L. Toupet, C. Andraud and O. Maury, *Org. Lett.*, 2008, **10**, 4159-4162.
118. Z. a. Li, Y. Liu, H. Kim, J. M. Hales, S.-H. Jang, J. Luo, T. Baehr-Jones, M. Hochberg, S. R. Marder, J. W. Perry and A. K. Y. Jen, *Adv. Mater.*, 2012, **24**, OP326-OP330.
119. Z. a. Li, H. Kim, S.-H. Chi, J. M. Hales, S.-H. Jang, J. W. Perry and A. K. Y. Jen, *Chem. Mater.*, 2016, **28**, 3115-3121.
120. H.-C. Lin, H. Kim, S. Barlow, J. M. Hales, J. W. Perry and S. R. Marder, *Chem. Commun.*, 2011, **47**, 782-784.

121. J. D. Matichak, J. M. Hales, S. Ohira, S. Barlow, S. H. Jang, A. K. Y. Jen, J. L. Brédas, J. W. Perry and S. R. Marder, *ChemPhysChem*, 2010, **11**, 130-138.
122. Z. a. Li, T. R. Ensley, H. Hu, Y. Zhang, S.-H. Jang, S. R. Marder, D. J. Hagan, E. W. Van Stryland and A. K. Y. Jen, *Adv. Optical Mater.*, 2015, **3**, 900-906.
123. M. R. Ferdinandus, M. Reichert, T. R. Ensley, H. Hu, D. A. Fishman, S. Webster, D. J. Hagan and E. W. Van Stryland, *Opt. Mater. Express*, 2012, **2**, 1776-1790.
124. J. D. Matichak, J. M. Hales, S. Barlow, J. W. Perry and S. R. Marder, *J. Phys. Chem. A*, 2011, **115**, 2160-2168.
125. M. Dinu, F. Quochi and H. Garcia, *Appl Phys Lett*, 2003, **82**, 2954-2956.
126. A. Eisfeld and J. S. Briggs, *Chem. Phys.*, 2002, **281**, 61-70.
127. V. V. Shelkovnikov, F. A. Zhuravlev, N. A. Orlova, A. I. Plekhanov and V. P. Safonov, *J. Mater. Chem.*, 1995, **5**, 1331-1334.
128. F. Wuerthner, T. E. Kaiser and C. R. Saha-Moeller, *Angew. Chem. Int. Ed.*, 2011, **50**, 3376-3410.
129. E. E. Jelley, *Nature*, 1936, **138**, 1009-1010.
130. Z. Li, S. Mukhopadhyay, S. H. Jang, J. L. Bredas and A. K. Jen, *J. Am. Chem. Soc.*, 2015, **137**, 11920-11923.

This journal is © The Royal Society of Chemistry 20xx

Please do not adjust margins

Table of Contents

The review reported recent progress of organic 2nd-order and 3rd-order nonlinear optical materials in Jen group.